Title

Localized High-Concentration Sulfone Electrolytes for High-Efficiency Lithium-Metal Batteries

Journal

Chem, 4(8)

ISSN

1925-6981

Authors

Ren, Xiaodi
Chen, Shuru
Lee, Hongkyung
et al.

Publication Date

2018-08-01

DOI

10.1016/j.chempr.2018.05.002

Peer reviewed

Chem

CellPress

Article

Localized High-Concentration Sulfone Electrolytes for High-Efficiency Lithium-Metal Batteries

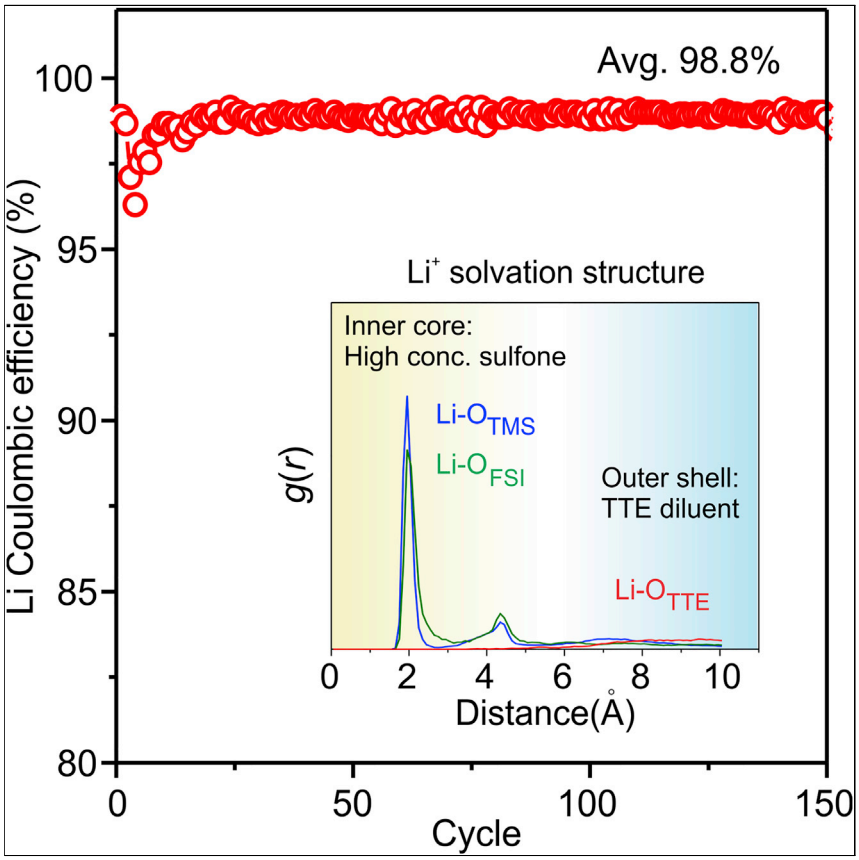

High-voltage batteries with Li-metal anodes can offer desirable high energy densities. Despite their excellent oxidative stability, sulfones have various limitations to be useful in Li-metal batteries, in particular their instability with Li metal. Here, we achieved a high Li Coulombic efficiency of nearly 99% in a sulfone-based localized high-concentration electrolyte (LHCE) with the addition of a non-solvating co-solvent. In addition, this co-solvent is highly beneficial for realizing stable battery cycling up to 4.9 V.

Xiaodi Ren, Shuru Chen, Hongkyung Lee, ..., Jun Liu, Ji-Guang Zhang, Wu Xu

jiguang.zhang@pnnl.gov (J.-G.Z.)
wu.xu@pnnl.gov (W.X.)

HIGHLIGHTS

Favorable electrolyte properties and solvation structures in sulfone-based LHCE

Improved Li-metal Coulombic efficiency in LHCE over HCE

Good AI protection for stable high-voltage battery cycling in LHCE

Ren et al., Chem 4, 1–16
August 9, 2018
https://doi.org/10.1016/j.chempr.2018.05.002

Please cite this article in press as: Ren et al., Localized High-Concentration Sulfone Electrolytes for High-Efficiency Lithium-Metal Batteries, Chem (2018), https://doi.org/10.1016/j.chempr.2018.05.002

Chem

CellPress

Article

Localized High-Concentration Sulfone Electrolytes for High-Efficiency Lithium-Metal Batteries

Xiaodi Ren,[1] Shuru Chen,[1] Hongkyung Lee,[1] Donghai Mei,[2] Mark H. Engelhard,[3] Sarah D. Burton,[3] Wengao Zhao,[1,4] Jianming Zheng,[1] Qiuyan Li,[1] Michael S. Ding,[5] Marshall Schroeder,[5] Judith Alvarado,[5,6] Kang Xu,[5] Y. Shirley Meng,[6] Jun Liu,[1] Ji-Guang Zhang,[1,*] and Wu Xu[1,7,*]

SUMMARY

To enable next-generation high-energy-density lithium (Li)-metal batteries (LMBs), an electrolyte that has simultaneous high Li-metal Coulombic efficiency (CE) and high anodic stability on cathodes is of significant importance. Sulfones are known for strong resistance against oxidation, yet their application in LMBs is restricted because of their poor compatibility with Li-metal anodes, high viscosity, and poor wettability. Here, we demonstrate that a high Li CE over 98% can be achieved in concentrated sulfone-based electrolytes. Furthermore, the viscosity and wettability issues of sulfones are resolved by the addition of a fluorinated ether, 1,1,2,2-tetrafluoroethyl-2,2,3,3-tetrafluoropropyl ether, to form a localized high-concentration electrolyte (LHCE), which not only provides further improvement in Li CE (98.8%) but also remains anodically stable with high-voltage cathodes, suppresses Al corrosion, and enables LMBs to operate in a wide temperature range. As a result, significantly improved cycling performance of LMBs has been realized with sulfone-based LHCE.

INTRODUCTION

With the surging demands for higher energy density batteries for portable electronic devices, electric vehicles, stationary energy storage, or large-scale grid implementations, the state-of-the-art lithium (Li)-ion batteries (LIBs) with a graphite anode (372 mAh g^{-1} theoretical specific capacity) and a lithium transition metal oxide cathode ($LiCoO_2$, $LiMn_2O_4$, $LiNi_xMn_yCo_{1-x-y}O_2$, etc.) fall short of expectations.[1,2] In order to increase the battery energy density, great attention has been paid to anodes and cathodes of larger electrochemical potential gaps to maximize the battery operation voltages as well as higher specific capacities. On the anode side, Li metal has been revived as an ideal anode material in the past few years because of its high theoretical specific capacity (3,862 mAh g^{-1}) combined with one of the lowest standard electrochemical potentials (−3.040 V).[3,4] However, there are enormous challenges in implementing Li-metal anodes, among which dendritic Li growth and low Li Coulombic efficiency (CE) are the most severe. Highly porous and dendritic Li deposition morphology due to the uncontrollable excessive side reactions between Li metal and electrolyte not only results in poor Li utilization and limited cycle life but also imposes serious safety threats because of the potential dendrite penetration through the separator. On the cathode side, the development of high-voltage (e.g., 5-V class) and high-capacity cathodes has attracted a lot of attention.[5,6] Apart from the discovery of new cathode materials of either higher voltage or of higher nickel content that are more catalytic, the most urgent task is to develop

The Bigger Picture

For high-voltage rechargeable lithium (Li)-metal batteries (LMBs), electrolytes with good stabilities on both the highly oxidative cathodes and the highly reductive Li-metal anodes are urgently desired. Sulfones have excellent oxidative stability, yet their high viscosity, poor wettability, and, in particular, incompatibility with Li anodes greatly hinder their applications in LMBs. Here, we demonstrate that a high Li Coulombic efficiency (CE) of 98.2% during repeated Li plating and stripping cycles can be realized in concentrated lithium bis(fluorosulfonyl)imide (LiFSI)-tetramethylene sulfone electrolyte. More importantly, the localized high-concentration electrolyte, formed by the dilution of the high-concentration electrolyte with a non-solvating fluorinated ether, 1,1,2,2-tetrafluoroethyl-2,2,3,3-tetrafluoropropyl ether, solves the viscosity and wettability issues, further improves Li CE (98.8%), and improves the high-voltage (4.9 V) performance of LMBs with effective Al protection.

electrolytes that have high anodic stability (>5.0 V) so that the desired cathode electrochemical processes can be supported reversibly, given that the carbonate solvents tend to decompose oxidatively beyond 4.5 V.[7,8] Among the promising solvents reported, sulfones stood out with particular stability against oxidation.[9] Xu and Angell[10] found that ethyl methyl sulfone (EMS) is stable up to 5.8 V even by a conservative evaluation. Seel and Dahn[11] used EMS as the electrolyte solvent to enable PF_6^- anion intercalation into graphene layers at 5.6 V. Good stability of sulfone electrolytes on the high-voltage $LiNi_{0.5}Mn_{1.5}O_4$ (LNMO) cathode has also been demonstrated.[12,13] In addition, sulfones have high dielectric constant and low flammability, both of which are desirable for battery applications.[14,15] However, sulfone-based electrolytes received limited research attention because they also have high melting points (typically above room temperature, except tetramethylene sulfone [TMS, or sulfolane], at 27°C), high viscosity, poor wettability toward electrodes and separators, and inability to form stable solid electrolyte interface (SEI) layers on graphite anodes.[16] For Li-metal batteries (LMBs), the side reactions of sulfones with Li metal are also problematic because of the high oxidation state of sulfur (S^{6+}) and the highly reductive nature of Li. Stable and efficient cycling of Li-metal anodes in sulfone-based electrolytes has not been reported so far.

In the last 5 years, a lot of progress has been made in stabilizing Li-metal anodes with concentrated electrolyte systems.[17–19] Increasing the salt-to-solvent molar ratio not only greatly reduces the amount of free solvent molecules and their chance of interacting with Li metal but also dramatically alters the interphasial chemistry on the Li surface. In a previous study, a high Li CE over 99% was achieved in the concentrated electrolytes of lithium bis(fluorosulfonyl)imide (LiFSI) in 1,2-dimethoxyethane (DME).[18] However, its practical application would still be difficult because of the ubiquitous issues associated with high-concentration electrolytes (HCEs), including the poor process capability in present cell manufacturing due to the high viscosity,[20] the poor wettability to separators and thick electrodes, the poor cell performances under low temperatures because of reduced ionic conductivities and increased liquidus line, and the high cost. In particular, the ether-based electrolytes are unable to withstand high-voltage cathode materials, thus limiting their wide applicability. These issues, with the exception of stability against high-voltage cathodes, would be even more problematic for sulfone-based electrolytes, which typically present higher viscosity and melting points above room temperature. Several attempts were made to solve these issues of HCEs by adding co-solvents.[21–25] Hydrofluoroether co-solvents have been added to concentrated lithium bis(trifluoromethanesulfonyl)imide (LiTFSI) in glymes or concentrated $LiBF_4$-propylene carbonate to reduce the electrolyte viscosity. It was indicated that hydrofluoroethers do not break the solvation structures in HCEs, thus maintaining the low polysulfide solubility[22] or the high anodic stability of HCEs.[23] More recently, our group have reported the introduction of a partially fluorinated ether, bis(2,2,2-trifluoroethyl) ether (BTFE), as a diluent to the HCEs of NaFSI in DME or LiFSI in dimethyl carbonate (DMC), which show improved performances on sodium-metal batteries or LMBs.[26,27] The obtained diluted electrolytes, although at lower apparent salt concentrations, seemed to have maintained all the desired properties for battery performance. Nevertheless, important questions remain regarding whether it is possible to stabilize Li-metal anodes with reactive sulfone molecules and which diluent is the best for concentrated sulfone electrolytes.

Here, we demonstrate that excellent Li stability can be realized in concentrated LiFSI-TMS electrolytes. More importantly, a non-solvating fluorinated ether, 1,1,2,2-tetrafluoroethyl-2,2,3,3-tetrafluoropropyl ether (TTE), was found to be the

[1]Energy and Environment Directorate, Pacific Northwest National Laboratory, Richland, WA 99354, USA

[2]Physical and Computational Sciences Directorate, Pacific Northwest National Laboratory, Richland, WA 99354, USA

[3]Environmental Molecular Sciences Laboratory, Pacific Northwest National Laboratory, Richland, WA 99354, USA

[4]School of Energy Research, Xiamen University, Xiamen, Fujian 361102, China

[5]Sensor and Electron Devices Directorate, US Army Research Laboratory, Adelphi, MD 20783, USA

[6]Department of NanoEngineering, Sustainable Power & Energy Center, University of California, San Diego, La Jolla, CA 92093, USA

[7]Lead Contact

*Correspondence: jiguang.zhang@pnnl.gov (J.-G.Z.), wu.xu@pnnl.gov (W.X.)

https://doi.org/10.1016/j.chempr.2018.05.002

Please cite this article in press as: Ren et al., Localized High-Concentration Sulfone Electrolytes for High-Efficiency Lithium-Metal Batteries, Chem (2018), https://doi.org/10.1016/j.chempr.2018.05.002

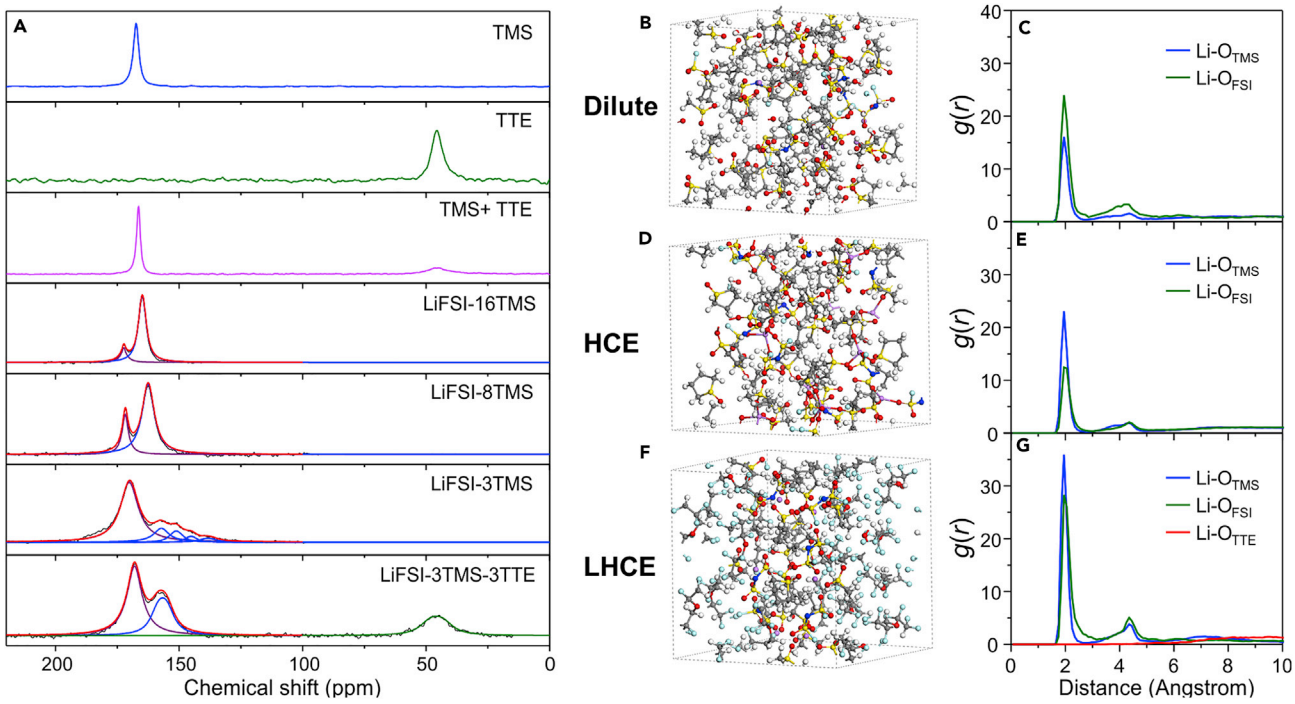

Figure 1. Experimental and Theoretical Studies of Electrolyte Solvation Structures

(A) Natural abundance ^{17}O-NMR spectra of different solvents and electrolytes collected at 60°C (333 K).

(B, D, and F) AIMD simulation snapshots of (B) dilute electrolyte (LiFSI-8TMS), (D) HCE electrolyte (LiFSI-3TMS), and (F) LHCE electrolyte (LiFSI-3TMS-3TTE) at 303 K.

(C, E, and G) Radial distribution functions $g(r)$ of Li-O_{FSI}, Li-O_{TMS}, and Li-O_{TTE} pairs calculated from AIMD simulation trajectories at 303 K in (C) dilute electrolyte, (E) HCE electrolyte, and (G) LHCE electrolyte.

best diluent, because it induced the formation of a stable, localized high-concentration electrolyte (LHCE). Not only does this sulfone-based LHCE have lower viscosities and higher ionic conductivities at lower temperatures as well as better wettability than the high-concentration sulfone electrolyte, thus enabling battery operation to sub-zero conditions (−10°C), but it also improves the efficiency of Li-metal anodes by suppressing their side reactions with TMS solvent molecules. Beyond that, better cycling stability of high-voltage (4.9 V) LMBs with LNMO cathodes can be realized with effective protection of Al current collector induced by the TTE diluent.

RESULTS AND DISCUSSION

Solvation Structure and Physical Properties

The effect of TTE addition on the electrolyte solvation structure was studied by natural abundance ^{17}O-nuclear magnetic resonance (NMR) (Figure 1A). When the LiFSI/TMS molar ratio increases from 1:16 to 1:8 and then to 1:3, the ^{17}O signal of sulfonyl oxygen atoms in FSI^- anion gradually shifts from 172.4 to 171.8 and then to 170.1 ppm. This is most likely due to the increased ion-dipole interactions between Li^+ and O atoms in FSI^- when the LiFSI concentration increases.[28] The ^{17}O signal of sulfonyl oxygen atoms in TMS also moves from 164.9 to 162.6 ppm, and even lower chemical shifts, indicating that the amount of TMS molecules coordinated with Li^+ is increasing. Nevertheless, when the LiFSI concentration is too high, Li^+ cannot be fully solvated by TMS molecules, and entry of FSI^- into the Li^+ solvation sheath becomes inevitable, forming a variety of solvation/complex structures (e.g., contact ion pairs and cation-anion aggregates).[17] In the HCE (LiFSI-3TMS), a very broad signal in the chemical shift range

Please cite this article in press as: Ren et al., Localized High-Concentration Sulfone Electrolytes for High-Efficiency Lithium-Metal Batteries, Chem (2018), https://doi.org/10.1016/j.chempr.2018.05.002

from 138.0 to 158.0 ppm appears for the oxygen atoms in TMS, which is tentatively fitted into a series of peaks to reflect different Li^+ solvation structures. When a non-solvating solvent TTE was added as a diluent, neither sulfonyl oxygen atoms in TMS and FSI^- shift back to the same positions as those in the low-concentration electrolytes (LiFSI-16TMS and LiFSI-8TMS). In contrast, the oxygen atoms in FSI^- show a further up-field shift to 170.1 from 168.1 ppm, and the signal of oxygen atoms in TMS at 156.7 ppm becomes much sharper. Because TTE is well miscible with TMS but has minimal interaction with either Li^+ or FSI^- (supported by theoretical results; Figure S1), it is likely that the TTE addition only separates large ion clusters in the HCE electrolyte while not disturbing the strong interactions between Li^+ and FSI^-. As a result, a heterogeneous electrolyte structure is likely to occur in the LHCE (LiFSI-3TMS-3TTE), with regions of concentrated electrolyte surrounded by TTE molecules, similar to the LHCEs of LiFSI-$(DMC)_m$-$(BTFE)_n$.

To understand the effect of the second electrolyte solvent TTE on the microscopic structures of LiFSI/TMS mixtures, three salt/solvent mixtures, i.e., two binary LiFSI/TMS mixtures (5LiFSI + 40TMS; 10LiFSI + 30TMS) and one ternary LiFSI/TMS/TTE (6LiFSI + 18TMS + 18TTE) mixture, were investigated by *ab initio* molecular dynamics (AIMD) simulations. The initial structure of each liquid salt/solvent mixture system was set up by randomly placing the numbers of LiFSI, TMS, and TTE molecules on the basis of experimental densities and molar ratios (concentration). The size of the simulation system is 20 × 20 × 20 Å. These initial structures were first relaxed by a home-made classic molecular dynamics simulation method with the flexible force field.[29,30] Upon quasi-equilibration of the system, a total of 15 ps AIMD simulation was carried out for each mixture system. The snapshots of the three salt/solvent mixture systems from AIMD summations are shown in Figures 1B, 1D, and 1F. They clearly demonstrate that all LiFSI salt molecules are closely coordinated with TMS instead of TTE. The last 5 ps AIMD simulation trajectories were used to calculate the radial distribution functions of Li-O_{TMS} and Li-O_{TTE} pairs. A sharp peak of the Li-O_{TMS} pair is identified at 1.95 Å for all three systems studied (Figures 1C, 1E, and 1G), indicating that all LiFSI salts are surrounded by TMS solvent molecules as the first coordination shell. This is due to the strong attractive interaction between TMS and LiFSI. Meanwhile TTE molecules are found to be barely coordinated with Li^+ in the ternary mixture system (Figure 1G). This clearly indicates that the localized high concentration of LiFSI/TMS pairs indeed exists, independent of the concentration of the second solvent TTE molecules.

The effects of the TTE diluent on the physical properties of the concentrated TMS electrolyte were studied by measuring the electrolytes' viscosity and ionic conductivity at different temperatures. As shown in Figure 2A, the HCE (LiFSI-3TMS) shows a high viscosity of 99.5 cP at 25°C. The electrostatic interactions are significantly increased compared with those of the conventional electrolytes at 1 M concentration because of the ion pairs and ion clusters in the electrolyte. The viscosity further increases when the temperature decreases, to 213 cP at 10°C and 775 cP at 0°C, both being much higher than that of the dilute electrolyte (LiFSI-8TMS). As indicated by differential scanning calorimetry (DSC) measurements (Table S1), both the liquidus point (28.2°C) and the precipitation point (−17.3°C) of the LiFSI-3TMS electrolyte are much higher than those of the LiFSI-8TMS electrolyte: −7.0°C and −41.4°C, respectively. In contrast, the LHCE (LiFSI-3TMS-3TTE) has a liquidus point of −35.3°C and a glass transition temperature of −113.4°C without a precipitation in cooling under conditions favorable to the precipitation. In addition, the viscosity of the LHCE is only 14.1 cP at 25°C and 51.2 cP at −10°C with the addition of TTE diluent, significantly lower than that of the concentrated LiFSI-3TMS electrolyte.

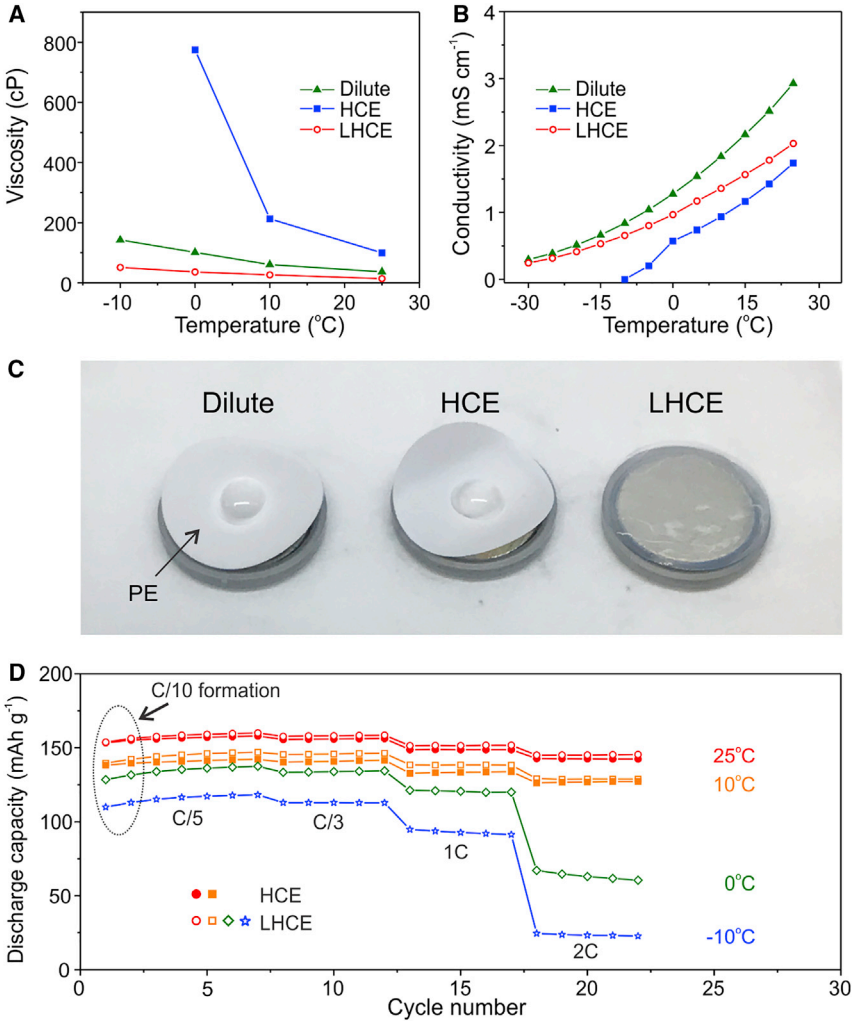

Figure 2. Physcial Properties and Low-Temperature Performances of Sulfone-Based Electrolytes
(A and B) Viscosity (A) and ionic conductivity (B) of sulfone-based electrolytes under different temperatures.
(C) Wettability tests of sulfone electrolytes on polyethylene (PE) separator.
(D) Comparison of discharge rate capabilities in HCE and LHCE at different temperatures (same charge rate at C/3 after twoformation cycles at C/10 rate).

Simultaneously, the ionic conductivity of the LiFSI-3TMS-3TTE is improved over a wide temperature range, whereas the LiFSI-3TMS electrolyte shows an apparent conductivity drop below 0°C (Figure 2B). According to the molar concentration, the viscosity, and the ionic conductivity data listed in Table S2, the Walden plot was made for the four electrolytes studied in this work (Figure S2). It was found that stronger ion associations exist in the electrolyte with increasing salt concentration, especially after TTE dilution. This agrees with the ^{17}O-NMR chemical shifts of FSI^- anions observed above and may have implications for electrolyte reactivity.

The poor wettability of sulfone-based electrolytes is also resolved with the presence of TTE. As shown in Figure 2C, neither LiFSI-8TMS nor LiFSI-3TMS electrolytes can effectively wet the polyethylene (PE) separator, whereas the TTE diluted electrolyte can easily spread over and soak the PE separator. Similar good wettability should be expected on both cathode and anode surfaces. With the enhanced ionic

Please cite this article in press as: Ren et al., Localized High-Concentration Sulfone Electrolytes for High-Efficiency Lithium-Metal Batteries, Chem (2018), https://doi.org/10.1016/j.chempr.2018.05.002

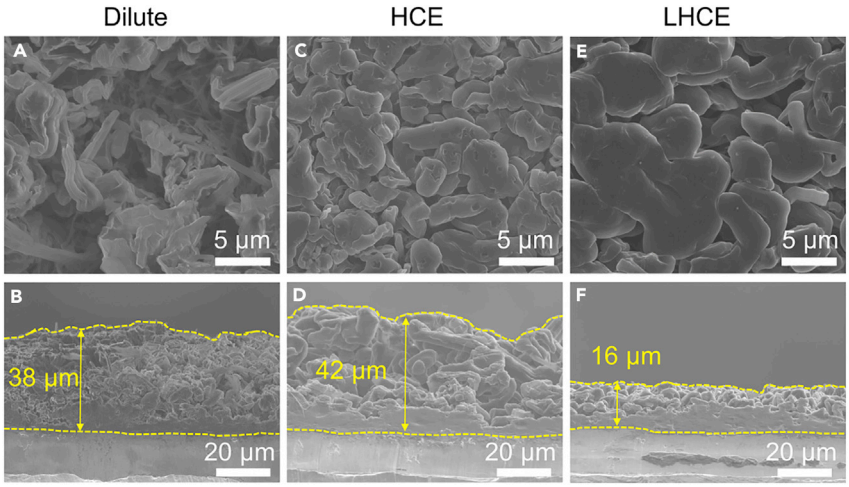

Figure 3. SEM Images of Li Deposition Morphologies in Different Sulfone Electrolytes
Dilute (A and B), HCE (C and D), and LHCE (E and F); both top-view (A, C, and E) and cross-section (B, D, and F) images are shown.

conductivity and wettability as well as the reduced viscosity, the LHCE of LiFSI-3TMS-3TTE demonstrates better rate capabilities in Li||$LiNi_{1/3}Mn_{1/3}Co_{1/3}O_2$ (Li||NMC) cells at different temperatures. As demonstrated in Figure 2D, although the cell using the HCE fails to operate at 0°C, the LHCE can still retain a large fraction of cell capacities at 1 C (1.5 mA cm^{-2}) or 2 C rates under 0°C or even −10°C. These results prove that the localized concentrated sulfone electrolyte can significantly improve its feasibility for practical applications.

Li-Metal Deposition Morphology and CE Measurement

The morphologies of the deposited Li metal were examined by the scanning electron microscopy (SEM) technique. The deposited Li film in the LiFSI-8TMS electrolyte shows an irregular growth and a highly porous structure with an average thickness around 38 μm (Figures 3A and 3B). The Li CE of the first cycle is only ~83.0% (Figure S3), which indicates excessive side reactions occurring between the low-concentration TMS electrolyte and Li metal. Apparently larger Li particles (2–8 μm) were deposited in the concentrated LiFSI-3TMS electrolyte, and the Li CE in the first cycle was improved to ~93.1%. Although this trend of particle size increase is similar to what was observed previously in the 4 M LiFSI/DME electrolyte,[18] the thickness of the deposited Li film is even higher (42 μm), and in the first cycle the Li CE is much lower in the concentrated sulfone electrolyte, suggesting a higher reactivity of TMS toward Li metal than DME. Interestingly, even larger Li particles in the order of 10 μm are formed in the LHCE and a much denser Li film 16 μm thick is obtained. The dense Li film with large particles has a reduced surface area and thus less tendency to react with the electrolyte. As a result, the first-cycle Li CE in the LHCE is greatly improved to 97.3%.

The Li-metal CE over long-term cycling can be studied by a repeated deposition and stripping method using the bare copper (Cu) foil as the substrate. As shown in our previous study, the Cu surface needs to be fully passivated before a stable Li CE can be observed.[31] Therefore, a Li film with an areal capacity of 5 mAh cm^{-2} was first deposited and then fully stripped. In the following cycles, 1 mAh cm^{-2} of Li metal was deposited and stripped to a cutoff voltage of 1 V. The same current density of 0.5 mA cm^{-2} was used throughout the cycling. The Li CE is the ratio of the stripped capacity to the deposited capacity. In Figure 4A, the Li CEs from cycling in different

Please cite this article in press as: Ren et al., Localized High-Concentration Sulfone Electrolytes for High-Efficiency Lithium-Metal Batteries, Chem (2018), https://doi.org/10.1016/j.chempr.2018.05.002

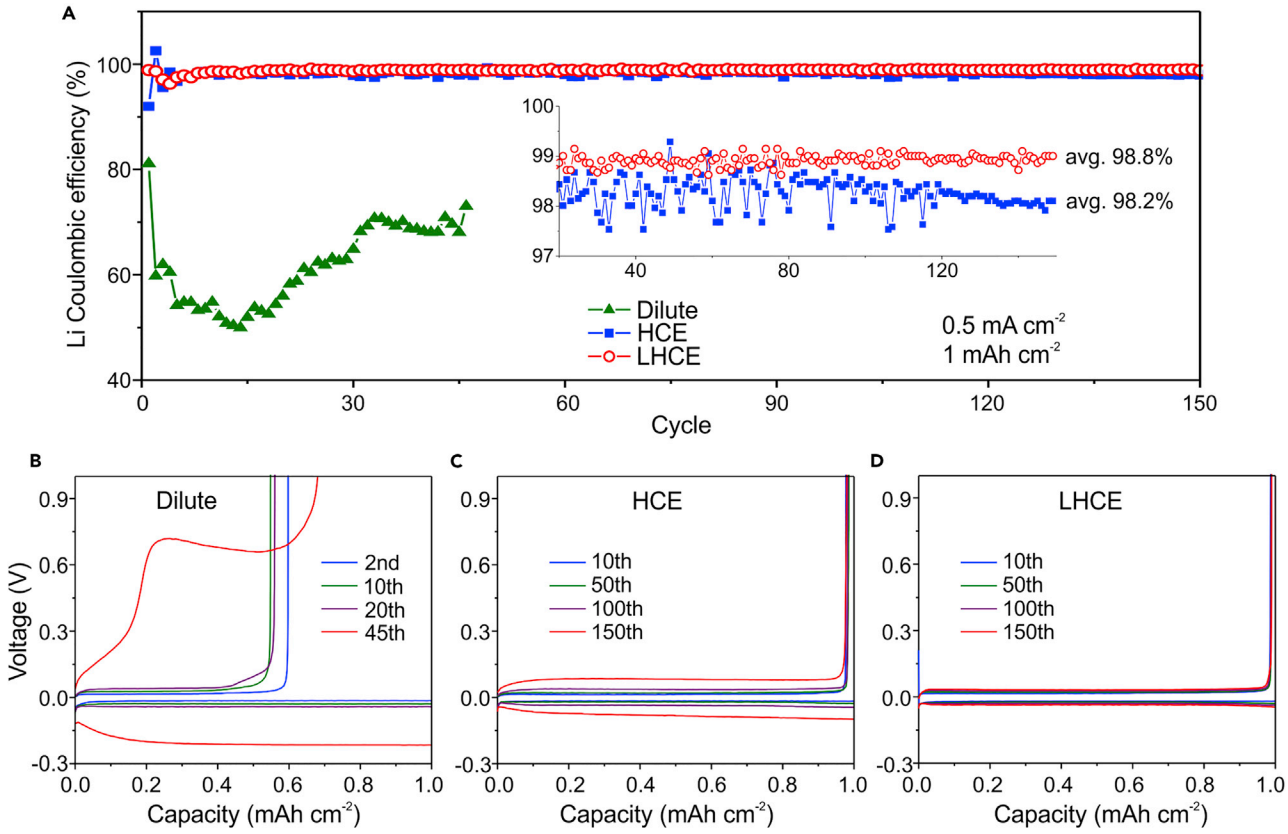

Figure 4. Li-Metal Cycling Behavior in Li||Cu Cells

(A) Li-metal CEs with cycling in different electrolytes measured in Li||Cu cells by repeated plating and stripping processes.

(B–D) Voltage profiles of Li plating and stripping processes at selected cycles in different sulfone electrolytes: (B) dilute, (C) HCE, and (D) LHCE.

electrolytes are compared. The Li CE in the dilute LiFSI-8TMS electrolyte shows a rapid drop to just ~50% in the first 20 cycles and the voltage gap between Li plating and stripping apparently increases (Figure 4B) as a result of a hike in cell impedance. This is in agreement with the porous and dendritic Li growth observed in Figure 3A and supports the fast accumulation of side reaction products between this electrolyte and Li metal. In the concentrated LiFSI-3TMS electrolyte, the Li-metal cycling CE is dramatically increased to ~98.2% and remains stable for over 150 cycles (Figure 4A). The voltage profiles are also much more stable with smaller hysteresis over the process (Figure 4C). This indicates that higher salt concentration effectively suppresses the side reactions between Li metal and TMS molecules. Despite the lower apparent salt concentration, the LHCE shows an even higher Li-metal CE, averaging over 98.8%, which remains more stable over the cycling. Meanwhile, the Li plating and stripping processes also show negligible polarization increase (Figure 4D) compared with those of the concentrated electrolyte (Figure 4C). These results along with the cycling tests of symmetric Li||Li cells (Figure S4) prove the remarkable enhancement of Li-metal stability brought about by the LHCE.

The choice of fluorinated ethers as the diluent is also critical for obtaining a stable LHCE with a heterogeneous solvation structure. Although most fluorinated ethers are miscible with the pure TMS solvent, several (e.g., ethyl 1,1,2,3,3,3-hexafluoropropyl ether, and perfluorobutyl ethyl pentyl ether) are found to be immiscible with the concentrated sulfone electrolyte (LiFSI-3TMS). It is likely that the

Please cite this article in press as: Ren et al., Localized High-Concentration Sulfone Electrolytes for High-Efficiency Lithium-Metal Batteries, Chem (2018), https://doi.org/10.1016/j.chempr.2018.05.002

complexation of TMS molecules with the LiFSI salt has greatly changed its interactions with fluorinated ethers. Although BTFE has a good miscibility with concentrated DME- or DMC-based electrolytes[26,27], it only has a limited miscibility with the concentrated TMS electrolyte. As shown in Figure S5, although the electrolyte containing LiFSI-3TMS-2BTFE is homogeneous, further dilution to LiFSI-3TMS-3BTFE causes clear phase separation. The differences might lie in the dielectric constants of different solvents. The dielectric constant can be an indicator of the polarity of a molecule. Both DME (ε = 7.2) and DMC (ε = 3.09) have close polarities with BTFE (whose dielectric constant is likely smaller than that of diethyl ether [ε = 4.33] according to Hougham et al.,[32] who reported that symmetric fluorine substitution for hydrogen decreases the dielectric constant of the parent molecule), but TMS has a much larger dielectric constant (ε = 42). It is likely that BTFE molecules have poor affinity to the LiFSI-TMS solvation outer sheath (presumably TMS molecules) in the LHCE, thus the interactions between the nearby LiFSI-TMS solvation complexes still dominate. On the other hand, TTE molecules, which have a higher dielectric constant (ε = 6.4) than BTFE, could have stronger interactions with the LiFSI-TMS solvation complexes to enable a stable heterogeneous electrolyte structure. We have not found phase separations in the LiFSI-TMS-TTE system. Furthermore, because of the continuous solvation/de-solvation processes taking place at the anode/electrolyte and the cathode/electrolyte interfaces during battery cycling, the ability of the diluent to maintain a stable electrolyte structure under dynamic conditions is critical for achieving desired battery performance. Compared with the dilution by TTE, the BTFE dilutions show apparently lower Li CEs (~98.1% for first 80 cycles), faster polarization increase, and shorter cycle life in Li||Cu cells (Figure S6). The insights on how solvent/diluent interactions affect Li-metal stability could provide important guidance for the future development of LHCEs.

Battery Cycling Performance with a Limited Li Anode

The excellent Li utilization in the LHCE can be further proved by cycling a limited amount of Li (50 μm thickness) with a moderately high loading NMC cathode (1.5 mAh cm^{-2}). In a conventional organic carbonate electrolyte used in LIBs, which has a composition of 1 M $LiPF_6$ in ethylene carbonate (EC) and ethyl methyl carbonate (EMC) (3:7 by vol.) with 2 wt % vinylene carbonate (VC), such a cell can just be cycled for about 50 cycles before a sudden failure occurs (Figure 5A). This is due to the severe reactions between Li metal and carbonate molecules and the depletion of both electrolyte and Li metal, as shown by the apparently increased cell polarization from voltage profiles (Figure S7). An even earlier cell capacity drop (less than 40 cycles) is seen in the dilute LiFSI-8TMS electrolyte, which indicates the higher reactivity between Li metal and sulfone. Nevertheless, significantly improved cycling stability over 300 cycles can be realized in both HCE (LiFSI-3TMS) and LHCE (LiFSI-3TMS-3TTE), which further proves the high Li CEs in these two electrolytes. When the cycled Li anodes were replaced with fresh Li metal after 300 cycles, neither of the cells showed capacity recoveries (Figure S8). It suggests that the observed gradual capacity fading should be attributed to the NMC cathode and that the anodes with limited amounts of Li metal are still functioning normally. Further analysis of the cycled NMC cathodes by X-ray diffraction (XRD) (Figure S9) shows the appearance of a lithiated spinel phase, $Li_2Mn_2O_4$. In addition, serious cracking of the secondary particles after 300 cycles was observed by SEM characterization (Figure S10), especially in the LiFSI-3TMS electrolyte. The exact reason for the cathode structural damage is still unclear and is beyond the scope of this work; however, it is likely due to the side reactions between the highly active cathode surface and the sulfone molecules, even though the average cell CEs are above 99.8% in both HCE and LHCE (Figure S11).

Please cite this article in press as: Ren et al., Localized High-Concentration Sulfone Electrolytes for High-Efficiency Lithium-Metal Batteries, Chem (2018), https://doi.org/10.1016/j.chempr.2018.05.002

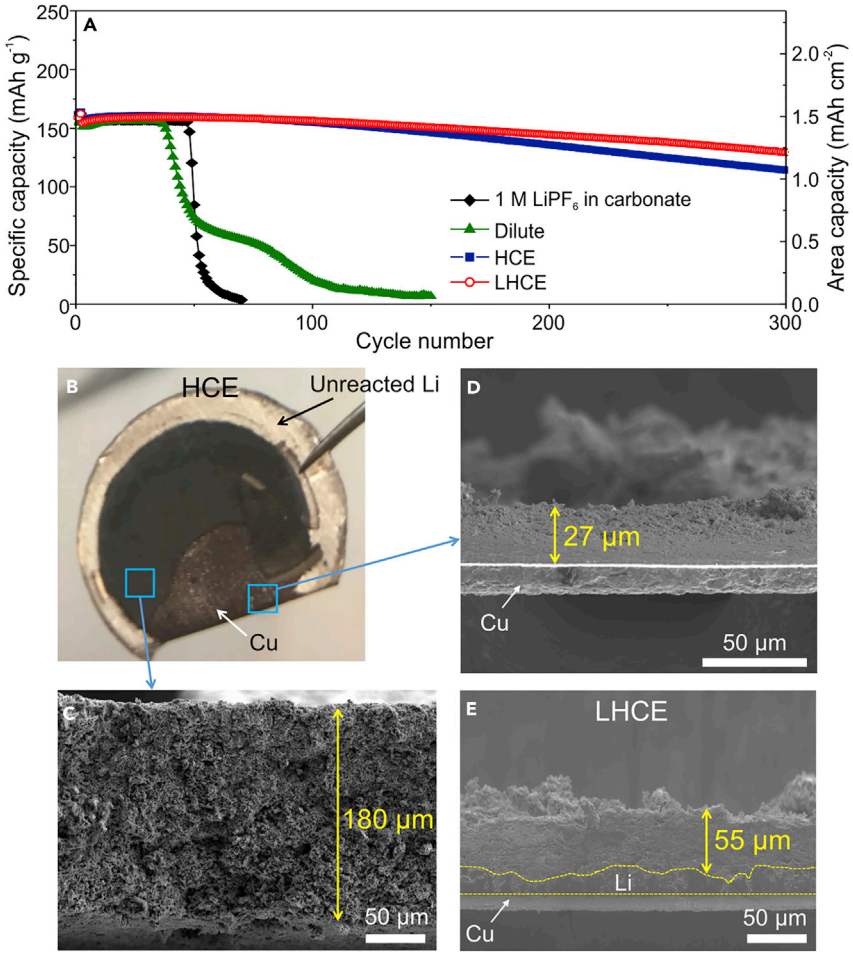

Figure 5. Li-Metal Cycling Behavior in Li||NMC Cells

(A) Comparison of cycling performances of Li||NMC cells using a 50-μm-thick Li anode and different electrolytes.

(B–D) The Li anode cycled in the HCE for 300 cycles: optical image (B), the cross-section SEM image of the top SEI layer (C), and the residual SEI layer on Cu foil (D).

(E) The cross-section SEM image of the Li anode cycled in the LHCE for 300 cycles.

Nevertheless, a significant difference was seen between the Li anodes cycled in the HCE and the LHCE. After 300 cycles in the HCE, the anode surface layer cracked and easily detached from the bulk Li anode when we were trying to prepare the cross-section sample for SEM analysis, exposing the Cu foil substrate underneath with barely any Li metal left (Figure 5B, the optical image). Further SEM characterizations indicate the total surface layer thickness is ~207 μm (180 + 27 μm, including the residual layer on the Cu substrate; Figures 5C and 5D), which is over four times higher than that of the pristine Li anode (50 μm). In contrast, the cross-section SEM image of the Li anode in the LHCE reveals a residual Li layer ~14–24 μm thick even after 300 cycles (Figure 5E). The dense anode after long-term cycling (~70 μm on average) suggests that Li-metal side reactions are remarkably suppressed and very efficient Li-metal CE is achieved in the sulfone-based LHCE.

Mechanisms of Enhanced Li-Metal Anode Stability

In order to further understand the high Li CE obtained, especially in the LHCE, X-ray photoelectron spectroscopy (XPS) equipped with argon ion sputtering was used to

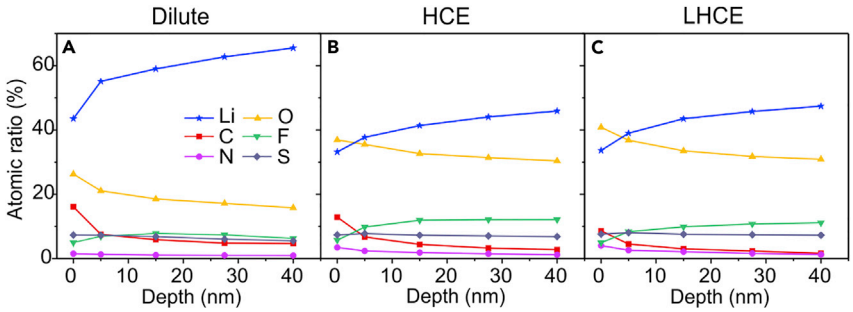

Figure 6. Variations of Elemental Distributions in the Li SEI Layers at Different Depths by XPS
Dilute (A), HCE (B), and LHCE (C). Li SEI layers were prepared on Cu substrate after ten plating and stripping cycles.

characterize the composition distribution of different elements in the Li SEI layers. The SEI layers were accumulated on Cu foils after ten plating and stripping cycles in different electrolytes (details in the Experimental Procedures). Remarkable differences in the elemental distributions in the Li SEI layers can be found for these three sulfone-based electrolytes (Figure 6). There are apparent enrichments of Li and C in the dilute electrolyte, implying a higher tendency of the side reactions between Li metal and the electrolyte during the SEI formation process and the follow-up cycling, especially the reactions with TMS solvent molecules. In addition, the F ratio is much lower than those in the HCE and the LHCE, indicating the Li metal reactions with LiFSI salt are preferred over the TMS solvent in concentrated electrolytes where the salt/solvent ratio is high. The elemental distribution features seen in the HCE and the LHCE are similar, which supports the belief that the addition of TTE co-solvent maintains the solvation structures in the LHCE as in the HCE. Interestingly, the C ratio is decreased with TTE addition, which is likely because of the further minimized side reactions between Li metal with the TMS molecules. As TTE is found to be much more inert toward Li than TMS (Figure S12), the decrease of TMS concentration with TTE dilution is beneficial for eliminating side reactions with Li metal.

The stability of various electrolyte components on Li metal can also be verified by density functional theory (DFT) calculations. The Li anode surface was represented by the Li(100) surface, which is the most stable among the three low-index surface structures, i.e., (100), (110), and (111) crystallographic planes.[33,34] The periodic Li(100) surface has a p(4 × 4) super cell with seven atomic Li layers. The optimized structures of TMS, TTE, LiFSI, and LiFSI/TMS and LiFSI/TTE pairs on the Li(100) surface are shown in Figure S13. Bader charge analysis[35] was performed to obtain the possible charge transfer between the electrolyte solvents and the salt species upon adsorption. DFT-calculated adsorption energies and Bader charges of each species are summarized in Table S3. Compared with TMS, LiFSI, and the LiFSI/TMS pair, the interaction between TTE and the Li surface is weak, suggesting that the TTE molecule is nearly inert and is barely reduced. However, TMS and the LiFSI/TMS pair are slightly reduced by obtaining the fractional charges of −0.22 and −0.40 |e|, respectively. This implies that both are possibly reduced and lead to interphasial ingredients originating from them. Comparing the projected densities of state of the three sulfone electrolytes on the Li surface (Figure S14), it is revealed that the lowest unoccupied molecular orbital (LUMO) energy level lies in the TMS solvent molecule in the dilute electrolyte, whereas in the HCE, the LUMO shifts to both LiFSI and TMS. This is consistent with the lower C ratio and higher F ratio detected in the HCE than in the dilute electrolyte. Furthermore, the LUMO energy level in the LHCE shifts to

Please cite this article in press as: Ren et al., Localized High-Concentration Sulfone Electrolytes for High-Efficiency Lithium-Metal Batteries, Chem (2018), https://doi.org/10.1016/j.chempr.2018.05.002

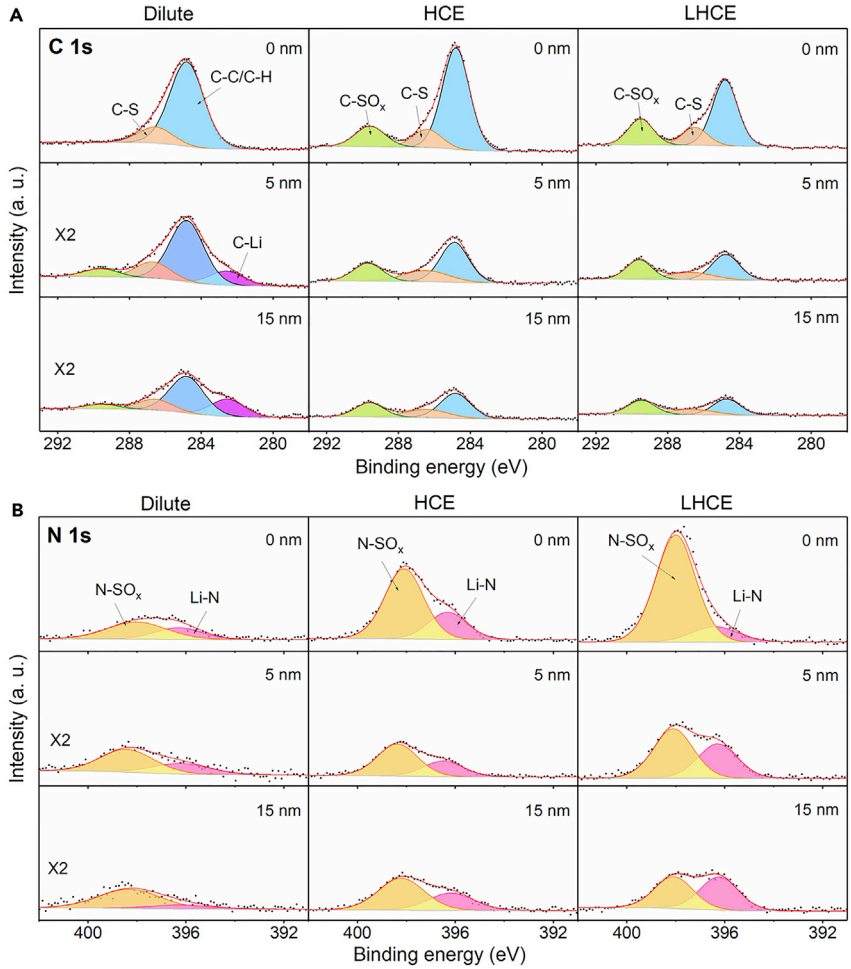

Figure 7. XPS Analysis of the SEI Compositions on Li-Metal Anodes

C 1s (A) and N 1s (B) spectra of the SEI layers on Cu substrates at different sputtering depths after ten plating and stripping cycles in the three sulfone-based electrolytes.

LiFSI, explaining the better inhibition of TMS decomposition and the interphase dominated by the reduction products from LiFSI.

The detailed formation mechanism of the interphase on Li was further studied by high-resolution XPS analysis. In the C 1s spectrum for the dilute electrolyte (Figure 7A), after the top SEI layer (mainly containing C–C/C–H and C–S species) was removed by sputtering, a peak at ~282.5 eV was detected, which can be ascribed to lithium carbides[36] and is likely from the reduction of TMS by Li metal. On the contrary, no carbides were detected in the HCE and the LHCE, supporting the suppression of solvent decomposition with a high salt/solvent ratio. The higher amount of LiF in the SEI layer also suggests the preferred reaction of LiFSI with Li in those two electrolytes (Figures 6 and S15). The N 1s spectra (Figure 7B) further reveal the difference of LiFSI reactions with Li in these three electrolytes. The N 1s peak at ~398.1 eV is most likely from N–SO_x species generated by incomplete decomposition of FSI^- anions, and the peak at 396.3 eV is attributed to Li-N species.[37] Although the N–SO_x species are dominant in the dilute electrolyte, the reactions between LiFSI and Li are much more complete in the concentrated electrolytes, especially in the LHCE, as indicated by the higher ratio of Li_xN observed in the inner SEI

Please cite this article in press as: Ren et al., Localized High-Concentration Sulfone Electrolytes for High-Efficiency Lithium-Metal Batteries, Chem (2018), https://doi.org/10.1016/j.chempr.2018.05.002

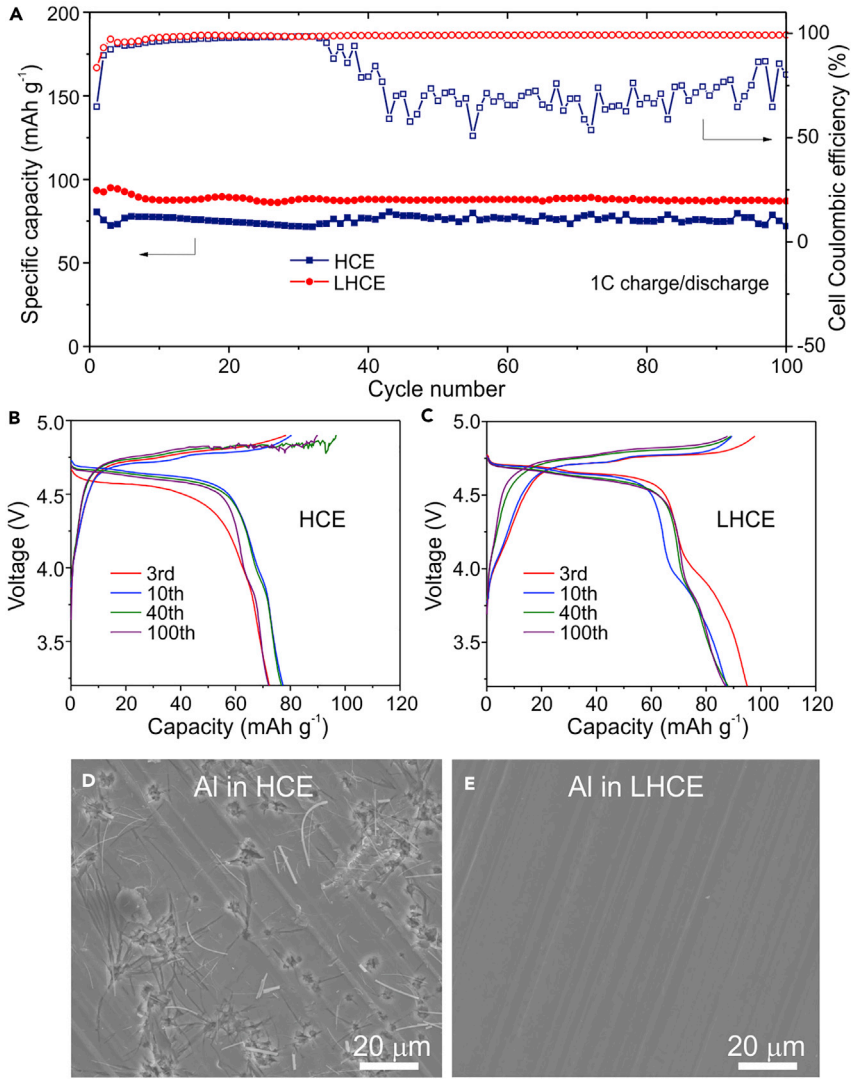

Figure 8. Electrochemical Behavior of Sulfone-Based Electrolyte in High-Voltage Li||LNMO Cells

(A) Discharge capacities and cell CEs of Li||LNMO cells in the HCE and the LHCE.

(B) Voltage profiles in the HCE.

(C) Voltage profiles in the LHCE (3.2–4.9 V; 1 C charge and discharge).

(D and E) SEM images of Al foils after tests in the HCE (D) and the LHCE (E).

layer. This also agrees with the higher reactivity of LiFSI on Li from DFT calculations. The enrichment of Li_xN, possibly Li_3N, whose Li^+ ionic conductivity is one of the highest among various SEI components (~2×10^{-4} to 4×10^{-4} S cm^{-1}),[38] is highly beneficial for reducing the resistance of the SEI layer. As a result, uniform Li plating and stripping processes can be achieved through the highly conductive and uniform SEI layer, thus decreasing the side reactions at the interface.

Effective Al Protection in LHCE

To study the high-voltage stability of the sulfone-based LHCE, LMBs with an LNMO cathode (2–3 mg cm^{-2} active material loading) were assembled and cycled with a high charge cutoff voltage at 4.9 V. As shown in Figure 8A, in the HCE electrolyte (2.75 m in molality), although the discharge capacity does not show obvious decay

Please cite this article in press as: Ren et al., Localized High-Concentration Sulfone Electrolytes for High-Efficiency Lithium-Metal Batteries, Chem (2018), https://doi.org/10.1016/j.chempr.2018.05.002

over cycling, unstable charging voltage profiles are observed after ~30 cycles above 4.83 V (Figure 8B). In the meantime, the average cell CE drops to below 70% after 40 cycles. Nevertheless, a stable cycling performance at 1 C charge/discharge rates can be realized in the LHCE with no voltage fluctuations (Figure 8C) and the average cell CE is kept over 99% after stabilization. The voltage fluctuations and low cell CE are likely caused by Al corrosion in the concentrated sulfone electrolyte. Pitting on the Al surface is observed after it is held at 5 V in the HCE (60°C, 7 days) (Figure 8D), which was reported very recently.[39] In contrast, the corrosion current on Al is largely diminished in the LHCE (Figure S16), and there are negligible changes on Al foil afterward (Figure 8E). Further XPS analysis (Figure S17) of the Al foils indicates that TTE molecules are involved in the formation of the protection layer on Al, which effectively suppresses further electrolyte decomposition and Al corrosion. This result proves that the addition of TTE diluent is beneficial under high voltages, and this sulfone-based LHCE is promising for high-voltage Li-metal battery applications.

Conclusions

We have demonstrated that stable and high-efficiency Li-metal cycling can be realized in sulfone-based electrolytes with the use of high salt concentrations in LiFSI-TMS electrolytes. More importantly, the formation of a stable LHCE with the addition of a non-solvating fluorinated ether (TTE) effectively addresses the high viscosity and poor wettability issues of the sulfone-based HCE. Experimental and theoretical studies show that TTE addition not only maintains the desired unique properties of the concentrated electrolytes but also further enhances the Li anode cycling efficiency, so that a very limited consumption of Li-metal anode was observed even after 300 cycles in Li||NMC cells. This sulfone-based LHCE significantly suppresses the decomposition of electrolyte on the Li anode and promotes the generation of a highly conductive SEI layer to enable high-efficiency Li-metal cycling. Furthermore, the LHCE solves the Al corrosion issue of concentrated LiFSI-sulfone electrolytes under high voltages, thus enabling stable cycling of Li||LNMO batteries at 4.9 V. This study paves the way for not only stabilizing sulfone-based electrolytes with Li-metal anode or other high-capacity anode materials but also enhancing battery performance under high-voltage conditions.

EXPERIMENTAL PROCEDURES

Materials

Battery-grade $LiPF_6$, EC, EMC, and VC were used as received from BASF Battery Materials (Independence, OH, United States). TMS was purchased from Sigma-Aldrich and further purified by distillation twice before being stored with molecular sieves to remove residual water (>99.9% purity estimated after purification). LiFSI (99%) was obtained from Nippon Shokubai and dried at 120°C overnight before use. TTE (99%, Synquest Laboratories) was also dried with molecular sieves. The LNMO material was synthesized as reported previously with a cooling rate of 5°C min^{-1}.[40] The NMC and LNMO cathodes were prepared by slurry coating at the Advanced Battery Facility at Pacific Northwest National Laboratory (PNNL) and dried at 120°C under vacuum before cell fabrication. The area of the NMC and LNMO cathode disks was 1.27 cm^2, and the material loading was about 1.5 mAh cm^{-2} for NMC and about 0.35 mAh cm^{-2} for LNMO.

Electrochemical Tests

Li CE was measured in Li||Cu cells, in which a piece of Cu foil (15 μm thick, 2.11 cm^2, All Foils), a separator, and a Li chip (250 μm thick, 1.56 cm^2, MTI Corporation) were sandwiched together in a CR2032 coin cell and crimped inside an argon-filled glovebox. A surfactant-coated separator (3501, Celgard) was used in cells with LiFSI-8TMS

Please cite this article in press as: Ren et al., Localized High-Concentration Sulfone Electrolytes for High-Efficiency Lithium-Metal Batteries, Chem (2018), https://doi.org/10.1016/j.chempr.2018.05.002

and LiFSI-3TMS electrolytes for better wettability; otherwise, a conventional PE separator was used. The SEI layers on Cu foils in Li||Cu cells were obtained by repeatedly depositing 1 mAh cm^{-2} of Li film and then fully stripping Li to 1 V for ten cycles (current density: 0.5 mA cm^{-2}). For Li||Li or Li||NMC cells, the Cu foil was replaced by a Li chip or a piece of NMC cathode. The cycling performances of Li||NMC cells with different electrolytes were evaluated within a voltage window of 2.7–4.3 V; the first two cycles were at a C/10 rate and then at C/3 for charge and discharge processes, where 1 C corresponded to a current density of 1.5 mA cm^{-2}. 75 μL of electrolyte was added in each coin cell for comparison.

Characterizations

Electrolyte viscosity measurements were carried out with a Brookfield DV2+ Pro Viscometer, which was equipped with a circulating bath for temperature control. Electrolyte conductivities were tested on a Bio-Logic MCS 10 fully integrated multichannel conductivity spectroscopy. The ^{17}O liquid state NMR spectra of the electrolytes were recorded on a 500 MHz Varian NMR Inova spectrometer with a Nalorac 5 mm dual-broadband probe tuned to 67.76 MHz. The 1d pulse sequence used incorporated a 15 μs 90° radiofrequency pulse, 50 ms acquisition time, and 0 .2 s recycle delay. All spectra were taken at 60°C, and 2,000 or 15,000 scans were collected on each sample. A differential scanning calorimeter (model DSC 2920, TA Instruments) was used to measure the liquidus points (thermodynamic upper limit of solid range) and the precipitation points (kinetic lower limit of liquid range) of the electrolytes.

For post analysis, tested coin cells were disassembled inside the glovebox to harvest the Cu substrates, Li foils, or NMC cathodes. These electrodes were thoroughly rinsed by fresh anhydrous DMC solvent to remove residual electrolytes and vacuum dried for further characterizations. SEM images were collected on an FEI Helios FE-SEM with an accelerating voltage of 5 kV, and the energy-dispersive X-ray (EDX) spectra were obtained with a voltage of 15 kV. XPS analysis was performed on a Physical Electronic Quantera scanning X-ray microprobe with a focused monochromatic Al Kα X-ray source. An Ar ion source was used for depth profiling at a 45° incident angle with 2 kV acceleration voltage. In order to avoid the interference from ambient atmosphere, samples were sealed in airtight containers before being transferred to the SEM and XPS instruments for analysis.

Theoretical Calculations

First-principles DFT and AIMD simulations were used to characterize the coordination in the studied sulfone-based electrolytes. All calculations were performed with the Vienna Ab Initio Simulation Package.[41–43] Electron-ion interactions were described by the projector-augmented wave pseudopotentials with the cutoff energy of 400 eV.[44,45] The exchange-correlation functional was represented by the Perdew-Burke-Ernzerhof generalized gradient approximation.[46] The exchange-correlation functional with a Gaussian smearing width term of 0.05 eV was used in the calculations of electrolytes and LiFSI salt interacting with Li-metal anode surface systems. The Monkhorst-Pack k-point mesh grid scheme (4 × 4 × 1) was used to obtain the optimized Li anode surface and the adsorption of electrolyte and salt molecules in the ground state. The convergence criteria for electronic self-consistent iteration and ionic relaxation were set to 1×10^{-6} and 1×10^{-4} eV, respectively. AIMD simulations of salt/solvent mixtures were performed in the canonical (NVT [number, volume, temperature]) ensemble at 303 K. The constant temperature of AIMD simulation systems was controlled via the Nose thermostat method with a Nose mass parameter of 0.5. The time step of 0.5 fs was used in all AIMD simulations.

A Monkhorst-Pack k-point mesh grid scheme (2 × 2 × 2) was used in AIMD simulations. The total AIMD simulation time for each salt/solvent system was 15 ps. The AIMD trajectory of the final 5 ps was used to obtain radial distribution functions of Li-O pairs.

SUPPLEMENTAL INFORMATION

Supplemental Information includes 17 figures and 3 tables and can be found with this article online at https://doi.org/10.1016/j.chempr.2018.05.002.

ACKNOWLEDGMENTS

This work was supported by the Assistant Secretary for Energy Efficiency and Renewable Energy of the US Department of Energy (DOE) Vehicle Technologies Office through the Advanced Battery Materials Research program (Battery500 Consortium) under contract no. DE-AC02-05CH11231. The SEM, EDX, XRD, XPS, and computational calculations were conducted in the William R. Wiley Environmental Molecular Sciences Laboratory, a national scientific user facility sponsored by the DOE Office of Biological and Environmental Research and located at the Pacific Northwest National Laboratory (PNNL). The PNNL is operated by Battelle for the DOE under contract no. DE-AC05-76RLO1830. The salt LiFSI was provided by Dr. Kazuhiko Murata of Nippon Shokubai Co., Ltd.

AUTHOR CONTRIBUTIONS

W.X., X.R., and J.-G.Z. proposed the research. W.X. and X.R. designed the experiments. X.R. performed the electrochemical measurements and conducted the SEM and EDX observations with help from S.C. and H.L. D.M. performed molecular dynamics simulations. M.H.E. performed XPS measurements. S.D.B. conducted the NMR measurements. W.Z. helped with XRD analysis. J.Z. synthesized the LNMO material. Q.L. prepared the NMC electrodes. M.S.D. carried out the DSC tests. M.S. and J.A. purified TMS solvent. All authors discussed the results. X.R. and W.X. prepared the manuscript with revisions by K.X., Y.S.M, J.L., and J.-G.Z. All authors gave approval to the final version of the manuscript.

DECLARATION OF INTERESTS

The authors declare no competing financial interests.

Received: February 6, 2018
Revised: April 22, 2018
Accepted: May 3, 2018
Published: June 14, 2018

REFERENCES AND NOTES

1. Manthiram, A. (2017). An outlook on lithium ion battery technology. ACS Cent. Sci. *3*, 1063–1069.

2. Goodenough, J.B., and Park, K.S. (2013). The Li-ion rechargeable battery: a perspective. J. Am. Chem. Soc. *135*, 1167–1176.

3. Cheng, X.B., Zhang, R., Zhao, C.Z., and Zhang, Q. (2017). Toward safe lithium metal anode in rechargeable batteries: a review. Chem. Rev. *117*, 10403–10473.

4. Xu, W., Wang, J., Ding, F., Chen, X., Nasybulin, E., Zhang, Y., and Zhang, J.-G. (2014). Lithium metal anodes for rechargeable batteries. Energy Environ. Sci. *7*, 513–537.

5. Whittingham, M.S. (2014). Ultimate limits to intercalation reactions for lithium batteries. Chem. Rev. *114*, 11414–11443.

6. Kraytsberg, A., and Ein-Eli, Y. (2012). Higher, stronger, better… a review of 5 volt cathode materials for advanced lithium-ion batteries. Adv. Energy Mater. *2*, 922–939.

7. Xu, K. (2014). Electrolytes and interphases in Li-ion batteries and beyond. Chem. Rev. *114*, 11503–11618.

8. Zhang, Z., Hu, L., Wu, H., Weng, W., Koh, M., Redfern, P.C., Curtiss, L.A., and Amine, K. (2013). Fluorinated electrolytes for 5 V lithium-ion battery chemistry. Energy Environ. Sci. *6*, 1806–1810.

9. Shao, N., Sun, X.G., Dai, S., and Jiang, D.E. (2011). Electrochemical windows of sulfone-based electrolytes for high-voltage Li-ion batteries. J. Phys. Chem. B *115*, 12120–12125.

10. Xu, K., and Angell, C.A. (1998). High anodic stability of a new electrolyte solvent: unsymmetric noncyclic aliphatic sulfone. J. Electrochem. Soc. *145*, L70–L72.

11. Seel, J.A., and Dahn, J.R. (2000). Electrochemical intercalation of PF_6 into graphite. J. Electrochem. Soc. *147*, 892–898.

12. Xue, L., Ueno, K., Lee, S.-Y., and Angell, C.A. (2014). Enhanced performance of sulfone-based electrolytes at lithium ion battery electrodes, including the $LiNi_{0.5}Mn_{1.5}O_4$ high voltage cathode. J. Power Sources *262*, 123–128.

13. Xue, L., Lee, S.-Y., Zhao, Z., and Angell, C.A. (2015). Sulfone-carbonate ternary electrolyte with further increased capacity retention and burn resistance for high voltage lithium ion batteries. J. Power Sources *295*, 190–196.

14. Xu, K., and Angell, C.A. (2002). Sulfone-based electrolytes for lithium-ion batteries. J. Electrochem. Soc. *149*, A920–A926.

15. Abouimrane, A., Belharouak, I., and Amine, K. (2009). Sulfone-based electrolytes for high-voltage Li-ion batteries. Electrochem. Commun. *11*, 1073–1076.

16. Xu, K. (2004). Nonaqueous liquid electrolytes for lithium-based rechargeable batteries. Chem. Rev. *104*, 4303–4418.

17. Yamada, Y., and Yamada, A. (2015). Review—superconcentrated electrolytes for lithium batteries. J. Electrochem. Soc. *162*, A2406–A2423.

18. Qian, J., Henderson, W.A., Xu, W., Bhattacharya, P., Engelhard, M., Borodin, O., and Zhang, J.G. (2015). High rate and stable cycling of lithium metal anode. Nat. Commun. *6*, 6362.

19. Fan, X., Chen, L., Ji, X., Deng, T., Hou, S., Chen, J., Zheng, J., Wang, F., Jiang, J., Xu, K., and Wang, C. (2018). Highly fluorinated interphases enable high-voltage Li-metal batteries. Chem *4*, 174–185.

20. Ding, M.S., von Cresce, A., and Xu, K. (2017). Conductivity, viscosity, and their correlation of a super-concentrated aqueous electrolyte. J. Phys. Chem. C *121*, 2149–2153.

21. Wang, H., Matsui, M., Kuwata, H., Sonoki, H., Matsuda, Y., Shang, X., Takeda, Y., Yamamoto, O., and Imanishi, N. (2017). A reversible dendrite-free high-areal-capacity lithium metal electrode. Nat. Commun. *8*, 15106.

22. Dokko, K., Tachikawa, N., Yamauchi, K., Tsuchiya, M., Yamazaki, A., Takashima, E., Park, J.W., Ueno, K., Seki, S., Serizawa, N., and Watanabe, M. (2013). Solvate ionic liquid electrolyte for Li-S batteries. J. Electrochem. Soc. *160*, A1304–A1310.

23. Doi, T., Shimizu, Y., Hashinokuchi, M., and Inaba, M. (2017). Dilution of highly concentrated $LiBF_4$/propylene carbonate electrolyte solution with fluoroalkyl ethers for 5-V $LiNi_{0.5}Mn_{1.5}O_4$ positive electrodes. J. Electrochem. Soc. *164*, A6412–A6416.

24. Moon, H., Mandai, T., Tatara, R., Ueno, K., Yamazaki, A., Yoshida, K., Seki, S., Dokko, K., and Watanabe, M. (2015). Solvent activity in electrolyte solutions controls electrochemical reactions in Li-ion and Li-sulfur batteries. J. Phys. Chem. C *119*, 3957–3970.

25. Ueno, K., Murai, J., Moon, H., Dokko, K., and Watanabe, M. (2017). A design approach to lithium-ion battery electrolyte based on diluted solvate ionic liquids. J. Electrochem. Soc. *164*, A6088–A6094.

26. Zheng, J., Chen, S., Zhao, W., Song, J., Engelhard, M.H., and Zhang, J.-G. (2018). Extremely stable sodium metal batteries enabled by localized high-concentration electrolytes. ACS Energy Lett. *3*, 315–321.

27. Chen, S., Zheng, J., Mei, D., Han, K.S., Engelhard, M.H., Zhao, W., Xu, W., Liu, J., and Zhang, J.G. (2018). High-voltage lithium-metal batteries enabled by localized high-concentration electrolytes. Adv. Mater. https://doi.org/10.1002/adma.201706102.

28. Wan, C., Hu, M.Y., Borodin, O., Qian, J., Qin, Z., Zhang, J.-G., and Hu, J.Z. (2016). Natural abundance ^{17}O, ^{6}Li NMR and molecular modeling studies of the solvation structures of lithium bis(fluorosulfonyl)imide/1,2-dimethoxyethane liquid electrolytes. J. Power Sources *307*, 231–243.

29. Han, S.D., Borodin, O., Seo, D.M., Zhou, Z.B., and Henderson, W.A. (2014). Electrolyte solvation and ionic association V. Acetonitrile-lithium bis(fluorosulfonyl)imide (LiFSI) mixtures. J. Electrochem. Soc. *161*, A2042–A2053.

30. Soetens, J.C., Millot, C., and Maigret, B. (1998). Molecular dynamics simulation of $Li(+)BF_4(-)$ in ethylene carbonate, propylene carbonate, and dimethyl carbonate solvents. J. Phys. Chem. A *102*, 1055–1061.

31. Adams, B.D., Zheng, J., Ren, X., Xu, W., and Zhang, J.-G. (2017). Accurate determination of coulombic efficiency for lithium metal anodes and lithium metal batteries. Adv. Energy Mater. *8*, 1702097.

32. Hougham, G., Tesoro, G., Viehbeck, A., and Chapple-Sokol, J.D. (1994). Polarization effects of fluorine on the relative permittivity in polyimides. Macromolecules *27*, 5964–5971.

33. Camacho-Forero, L.E., Smith, T.W., Bertolini, S., and Balbuena, P.B. (2015). Reactivity at the lithium-metal anode surface of lithium-sulfur batteries. J. Phys. Chem. C *119*, 26828–26839.

34. Doll, K., Harrison, N.M., and Saunders, V.R. (1999). A density functional study of lithium bulk and surfaces. J. Phys. Condens. Matter *11*, 5007–5019.

35. Henkelman, G., Arnaldsson, A., and Jonsson, H. (2006). A fast and robust algorithm for Bader decomposition of charge density. Comput. Mater. Sci. *36*, 354–360.

36. Aurbach, D., Gamolsky, K., Markovsky, B., Gofer, Y., Schmidt, M., and Heider, U. (2002). On the use of vinylene carbonate (VC) as an additive to electrolyte solutions for Li-ion batteries. Electrochim. Acta *47*, 1423–1439.

37. Olschewski, M., Gustus, R., Höfft, O., Lahiri, A., and Endres, F. (2017). Monochromatic X-ray photoelectron spectroscopy study of three different ionic liquids in interaction with lithium-decorated copper surfaces. J. Phys. Chem. C *121*, 2675–2682.

38. Lapp, T. (1983). Ionic conductivity of pure and doped Li_3N. Solid State Ionics *11*, 97–103.

39. Alvarado, J., Schroeder, M.A., Zhang, M., Borodin, O., Gobrogge, E., Olguin, M., Ding, M.S., Gobet, M., Greenbaum, S., Meng, Y.S., and Xu, K. (2018). A carbonate-free, sulfone-based electrolyte for high-voltage Li-ion batteries. Mater. Today. https://doi.org/10.1016/j.mattod.2018.02.005.

40. Zheng, J., Xiao, J., Nie, Z., and Zhang, J.G. (2013). Lattice Mn^{3+} behaviors in $Li_4Ti_5O_{12}$/$LiNi_{0.5}Mn_{1.5}O_4$ full cells. J. Electrochem. Soc. *160*, A1264–A1268.

41. Kresse, G., and Furthmuller, J. (1996). Efficient iterative schemes for ab initio total-energy calculations using a plane-wave basis set. Phys. Rev. B *54*, 11169–11186.

42. Kresse, G., and Hafner, J. (1993). Ab initio molecular-dynamics for liquid-metals. Phys. Rev. B *47*, 558–561.

43. Kresse, G., and Hafner, J. (1994). Ab initio molecular dynamics simulation of the liquid-metal amorphous-semiconductor transition in germanium. Phys. Rev. B *49*, 14251–14269.

44. Blochl, P.E. (1994). Projector augmented-wave method. Phys. Rev. B *50*, 17953–17979.

45. Kresse, G., and Joubert, D. (1999). From ultrasoft pseudopotentials to the projector augmented wave method. Phys. Rev. B *59*, 1758–1775.

46. Perdew, J.P., Burke, K., and Ernzerhof, M. (1996). Generalized gradient approximation made simple. Phys. Rev. Lett. *77*, 3865–3868.

Chem, Volume *4*

Supplemental Information

Localized High-Concentration Sulfone Electrolytes for High-Efficiency Lithium-Metal Batteries

Xiaodi Ren, Shuru Chen, Hongkyung Lee, Donghai Mei, Mark H. Engelhard, Sarah D. Burton, Wengao Zhao, Jianming Zheng, Qiuyan Li, Michael S. Ding, Marshall Schroeder, Judith Alvarado, Kang Xu, Y. Shirley Meng, Jun Liu, Ji-Guang Zhang, and Wu Xu

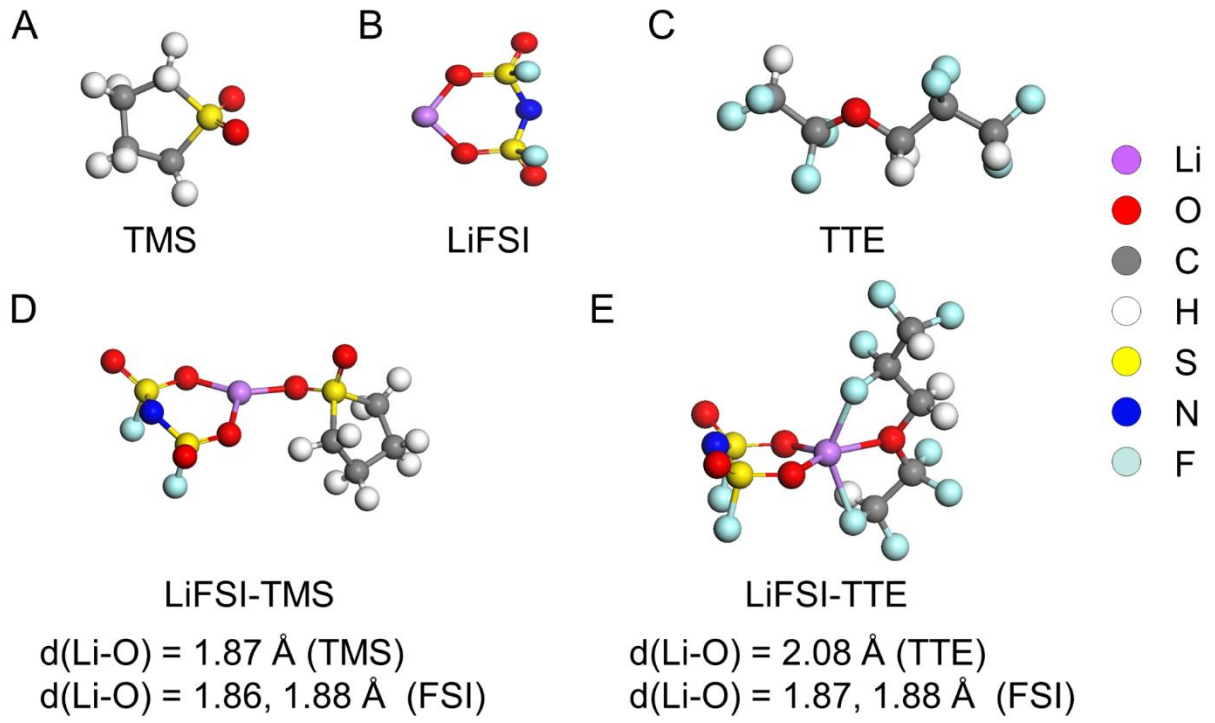

Figure S1. Optimized structures of TMS and TTE solvent molecules, LiFSI salt, and LiFSI-TMS, LiFSI-TTE solvent salt pairs.

Figure S1 shows the optimized geometries of TMS, TTE, LiFSI, and pairs of LiFSI/TMS and LiFSI/TTE in vacuum using VASP. Only Γ-centered k-point mesh was used for above calculations. Similar results were also obtained using the Gaussian 09 package with PBE and the 6-311++G(p,d) basis set.[1] It is found that LiFSI salt is preferentially coordinated with TMS via the Li-O_{TMS} bond. The Li-O_{TMS} bond length is 1.87 Å, which is the same as the Li-O_{FSI} bond length (1.87 Å), while the Li-O_{TTE} bond length is relative longer, as of 2.08 Å. This is also reflected by the stronger interaction between LiFSI and TMS than the interaction between LiFSI and TTE. The calculated interaction energy between LiFSI and TMS is -84.6 kJ·mol^{-1}, while the interaction between LiFSI and TTE is only -45.1 kJ·mol^{-1}.

Table S1. Liquidus and precipitation points of different sulfone electrolytes by DSC

Electrolyte	Liquidus point	Precipitation point
Dilute (LiFSI-8TMS)	-7 ºC	-41.4 ºC
HCE (LiFSI-3TMS)	28.2 ºC	-17.3 ºC
LHCE (LiFSI-3TMS-3TTE)	-35.3 ºC	-113.4 ºC

Table S2. The molar concentration, viscosity and conductivity data of the studied electrolytes

Electrolytes	Molarity (mol L^{-1})	Viscosity (cP)	Conductivity (mS cm^{-1})
1 M $LiPF_6$ in EC/EMC + 2% VC	1.0	3.83 (25°C), 7.02 (10°C), 9.87 (0°C), 13.2 (-10°C)	8.31 (25°C), 5.86 (10°C), 4.42 (0°C), 3.14 (-10°C)
LiFSI-8TMS	1.18	36.7 (25°C), 60.6 (10°C), 101.3 (0°C), 142.6 (-10°C)	2.93 (25°C), 1.84 (10°C), 1.28 (0°C), 0.84 (-10°C)
LiFSI-3TMS	2.62	99.5 (25°C), 213 (10°C), 775 (0°C)	1.74 (25°C), 0.94 (10°C), 0.57 (0°C)
LiFSI-3TMS-3TTE	1.20	14.1 (25°C), 26.5 (10°C), 36.1 (0°C), 51.2 (-10°C)	2.03 (25°C), 1.36 (10°C), 0.97 (0°C), 0.66 (-10°C)

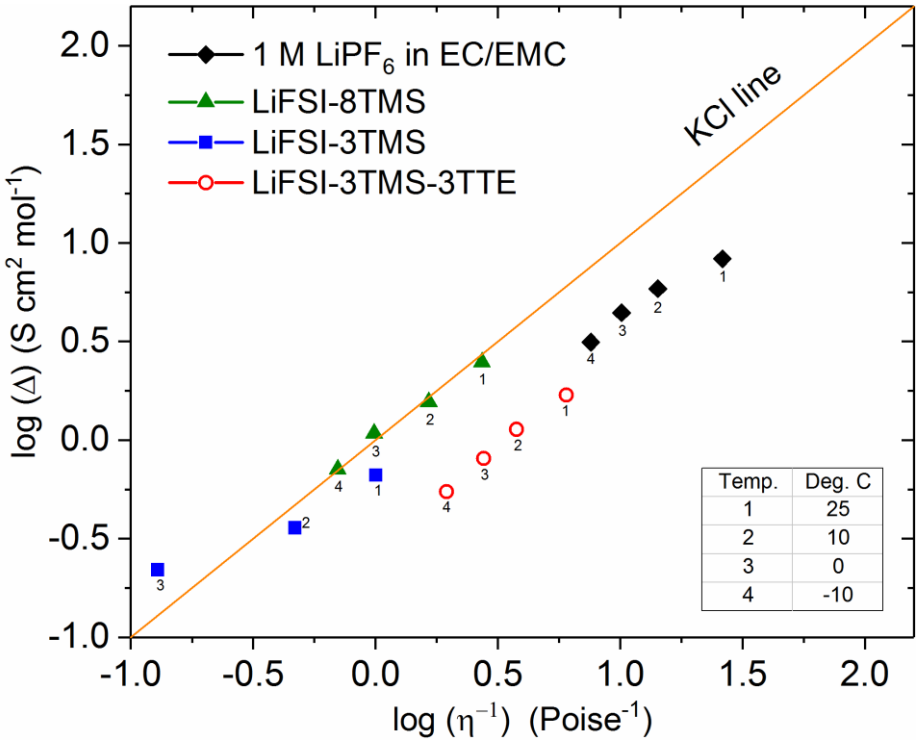

Figure S2. Walden plots for the four electrolytes studied in this work.

With the increase of the LiFSI/TMS mole ratio (i.e. the salt concentration), apparently stronger ion associations are observed, where the deviation at 0°C for LiFSI-3TMS is possibly related to salt precipitation at this temperature because the LiFSI-3TMS electrolyte has the liquidus point at 28.2°C and the precipitation point of -17.3°C according to the DSC measurement. Interestingly, even stronger ion associations are noticed in the LHCE (LiFSI-3TMS-3TTE). This could be explained by the unique heterogeneous electrolyte structure where LiFSI-TMS solvation complexes are separated by non-solvating fluorinated ether TTE molecules. Without the electrostatic interactions with other ions as in the concentrated electrolyte, Li^+ cations and FSI^- anions are likely to show stronger bindings with each other, thus stronger ion associations.

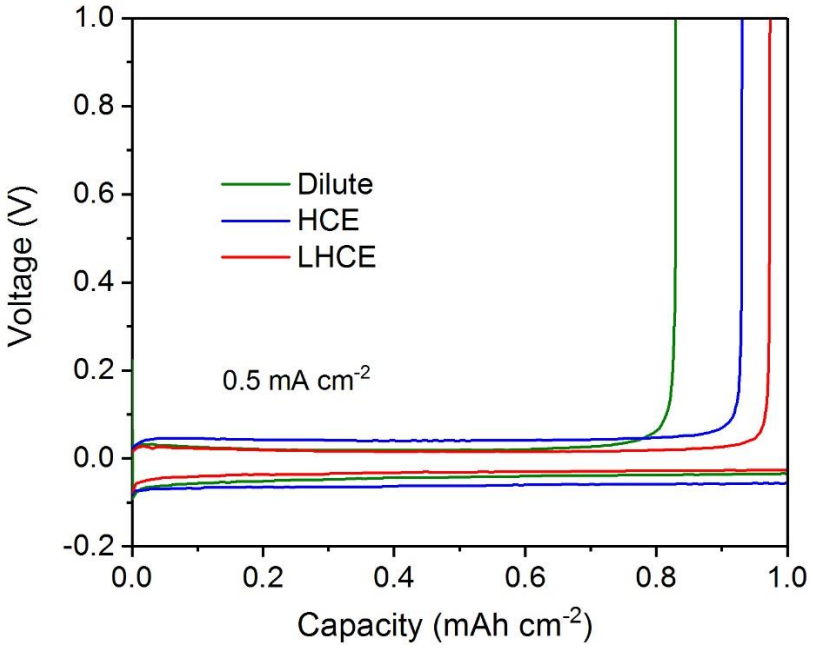

Figure S3. First cycle voltage profiles of Li plating/stripping in different sulfone electrolytes at a current density of 0.5 mA cm^{-2} and an area capacity of 1 mAh cm^{-2}.

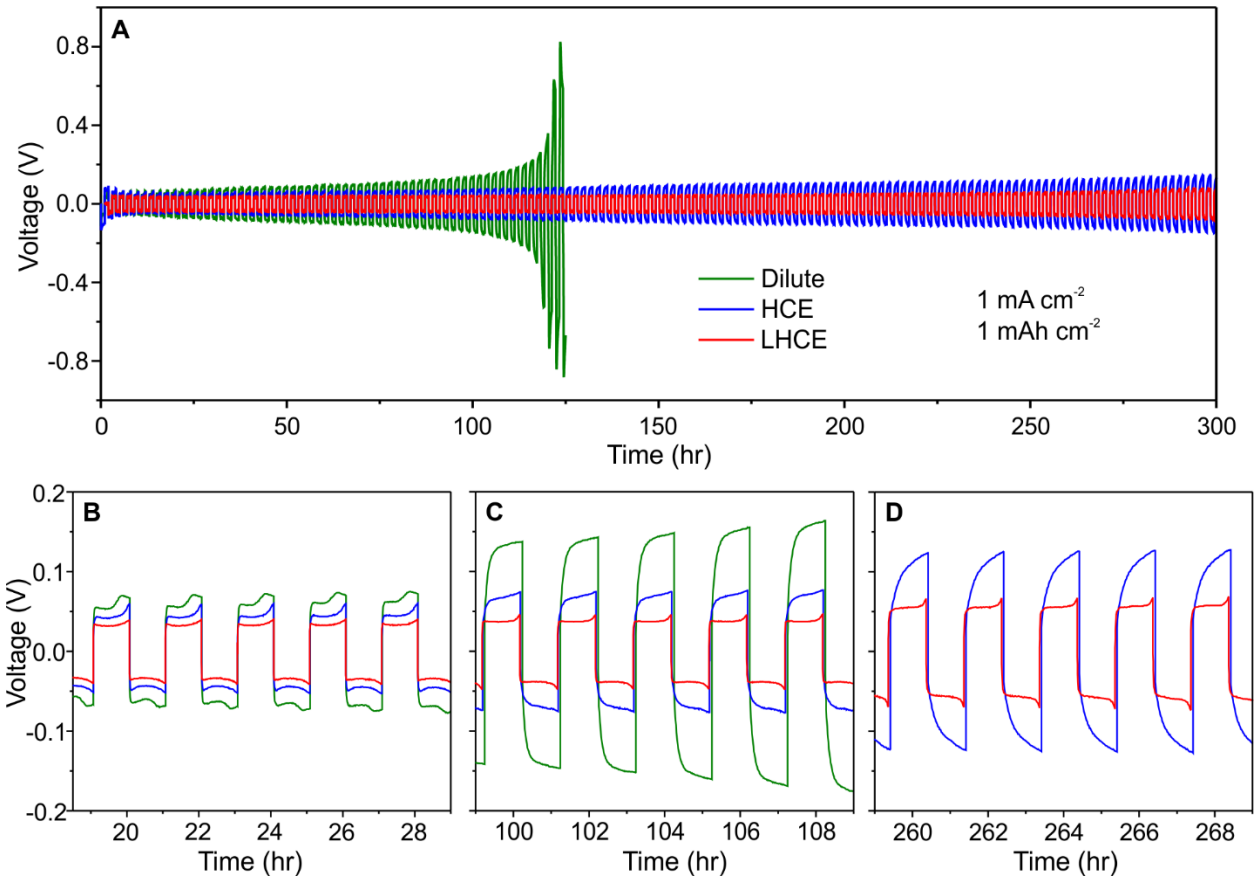

Figure S4. (A) Voltage profiles of symmetric Li||Li cells cycling in different sulfone electrolytes. (B-D) The enlarged voltage profiles at different stages.

The cycling stability of Li metal in the three studied sulfone-based electrolytes can also be evidenced by the evolutions of the cell voltage polarization in symmetric Li||Li cells during cycling. As indicated in Figure S4, the voltage profile evolutions in different electrolytes show significant differences. Because of the high reactivity between Li metal and TMS molecules, the cell polarization in the dilute electrolyte (LiFSI-8TMS) shows a fast increase and a sudden failure due to the similar issues of Li metal corrosion and electrolyte depletion. In contrast, the cell voltage profiles in the HCE (LiFSI-3TMS) and the LHCE (LiFSI-3TMS-3TTE) have greatly improved stability and minimal polarization increases over 300 h without short-circuiting. This is in

consistent with the previous results of high Li CE measured in Li||Cu cells, which means the accumulation of side reaction products is greatly reduced in these two electrolytes. In addition, this effect is more apparent in the LHCE. The initial voltage gap of the cell using the LHCE is smaller than that in the HCE because of its higher ionic conductivity. The difference becomes much more apparent with cycling, further supporting the minimized side reaction products built-up in the LHCE. Another feature of the LHCE is the very similar shape of the voltage profiles, implying the Li plating/stripping behavior is highly consistent over the long-term cycling. In contrast, the voltage profiles in the HCE change into arches after cycling. In previous studies, this "arching" behavior has been shown to be related to the Li^+ mass-transport issue due to the growth of the porous SEI layer. This proves the denser Li growth and more compact SEI layer formed in the LHCE is beneficial for protecting Li metal and maintaining the cell polarization on Li metal anode.

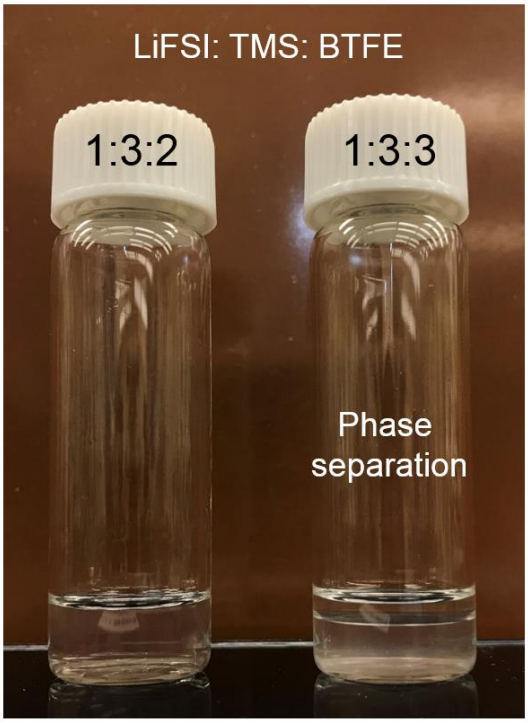

Figure S5. Appearance of the mixtures of concentrated LiFSI-3TMS electrolyte with BTFE at different dilution ratios. A clear phase separation is observed for the more diluted electrolyte.

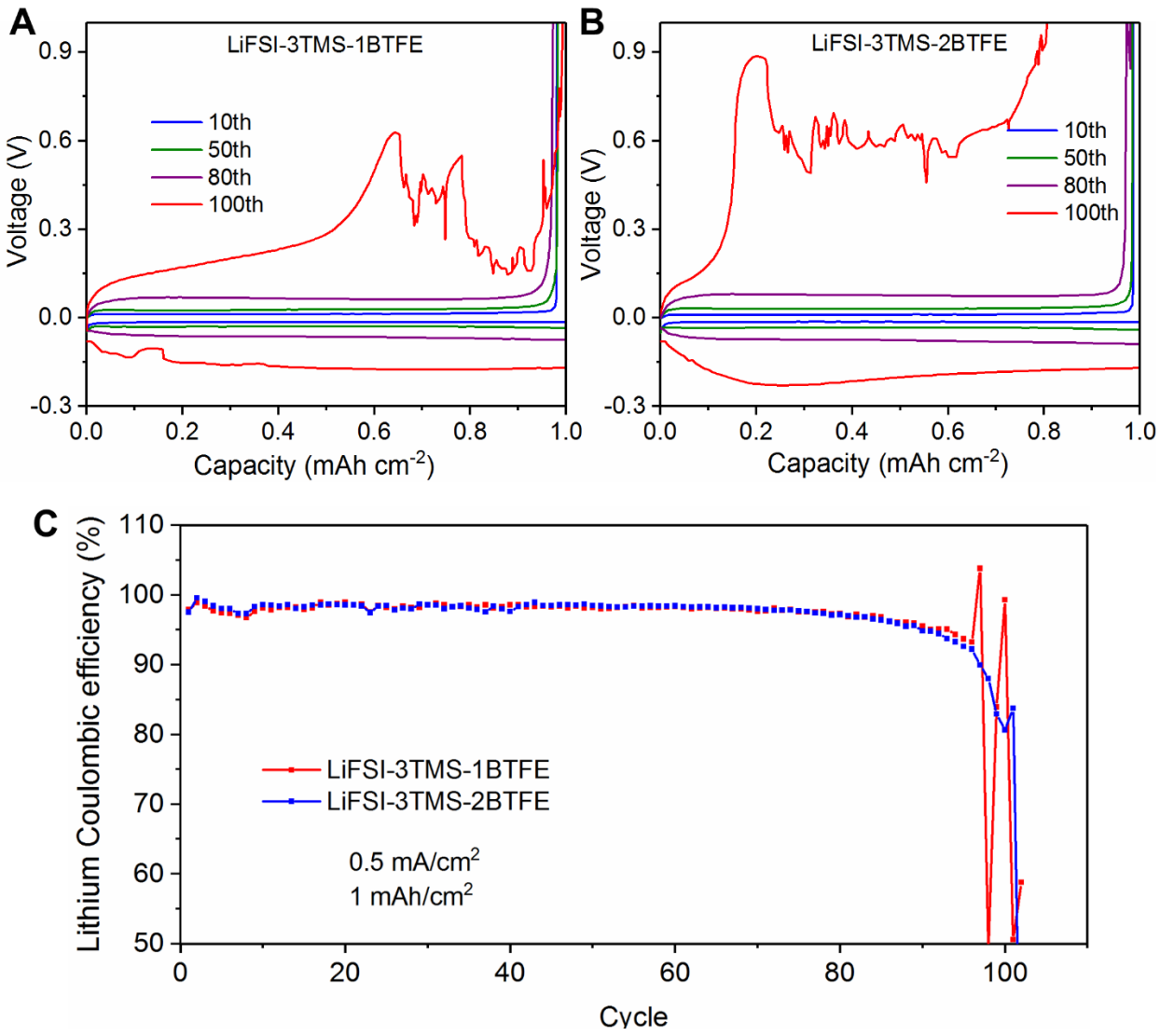

Figure S6. Tests of the Li||Cu cells with BTFE-diluted concentrated sulfone electrolytes. (A) Li plating/stripping voltage profiles in the LiFSI-3TMS-1BTFE electrolyte. (B) Li plating/stripping voltage profiles in the LiFSI-3TMS-2BTFE electrolyte. (C) The comparison of Li CE with cycling in the two electrolytes.

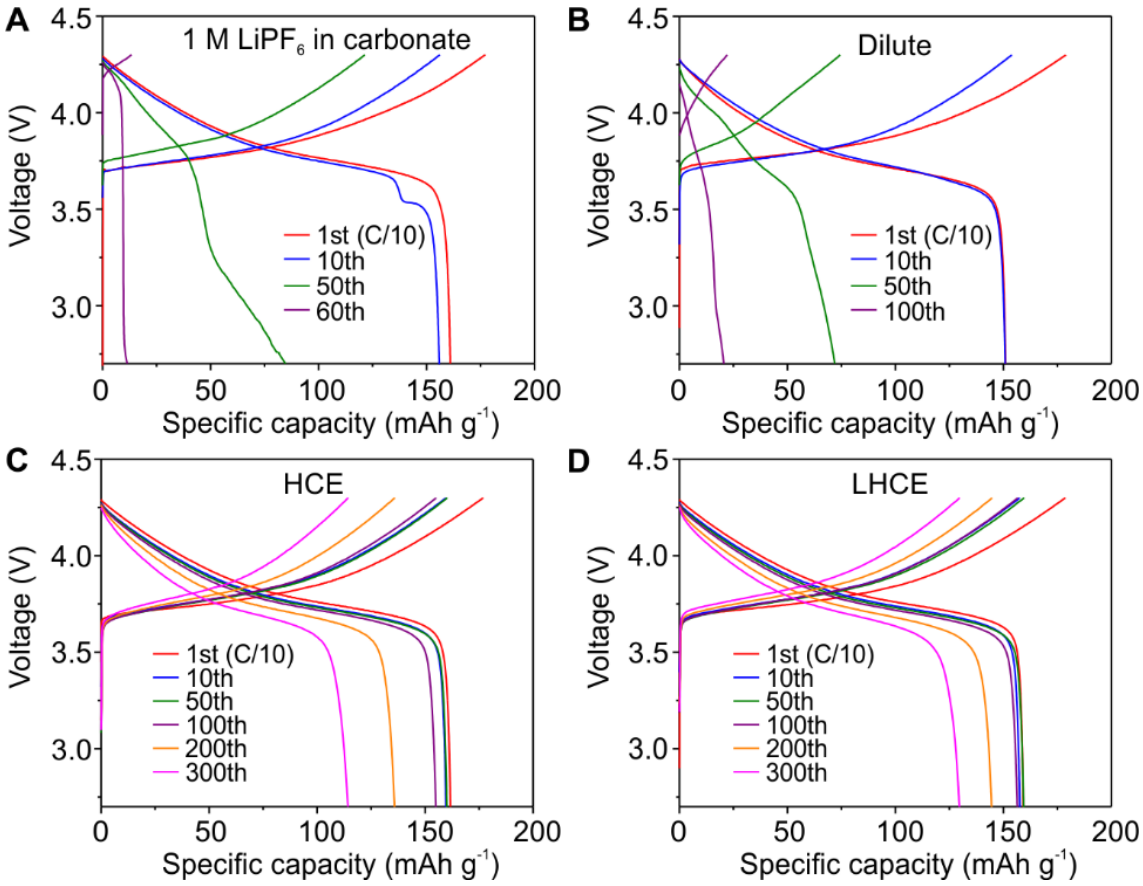

Figure S7. Voltage profiles of Li||NMC cells with 50 µm thick Li in different electrolytes: (A) 1 M $LiPF_6$ in EC/EMC (3:7 by vol.) with 2 wt% VC, (B) LiFSI-8TMS, (C) LiFSI-3TMS, (D) LiFSI-3TMS-3TTE.

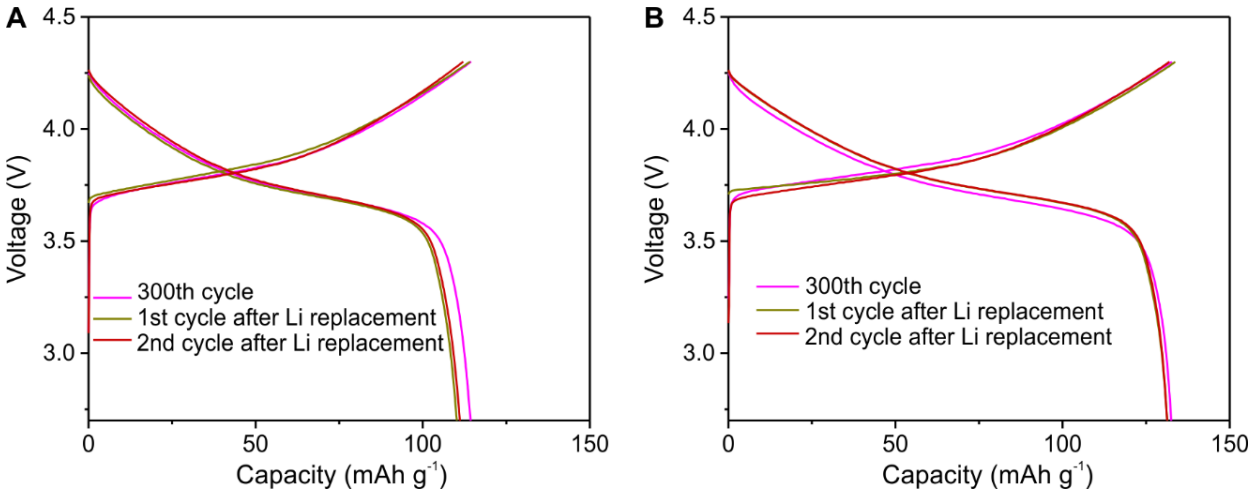

Figure S8. Voltage profiles of Li||NMC cells with new Li anodes and cycled NMC cathodes (300 cycles) in (A) LiFSI-3TMS electrolyte and (B) LiFSI-3TMS-3TTE electrolyte.

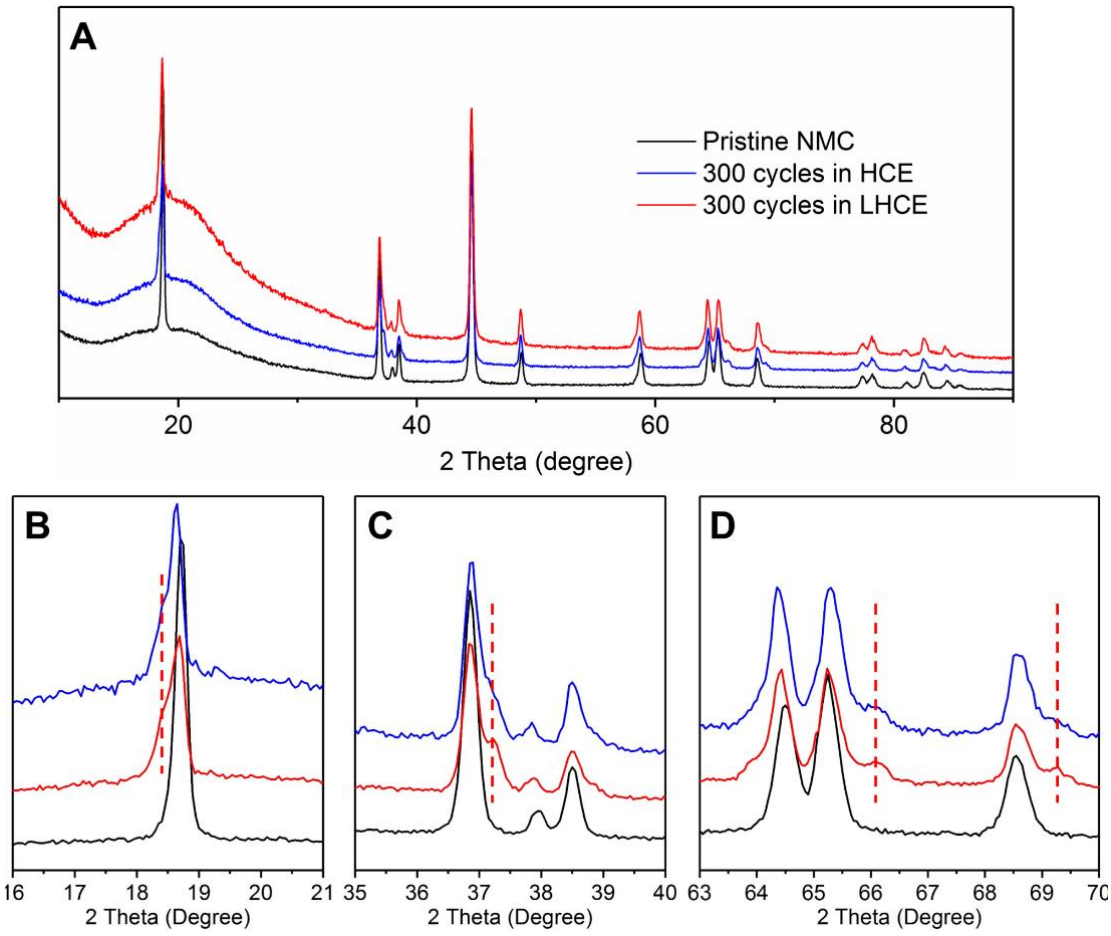

Figure S9. (A) XRD patterns of the pristine NMC cathode and the cathodes after 300 cycles in the HCE and the LHCE. (B-D) Enlarged patterns in different regions. (New XRD peaks evolved after cycling are marked by dotted lines, which are assigned to the new $Li_2Mn_2O_4$ phase (JCPDF No. 38-0299))

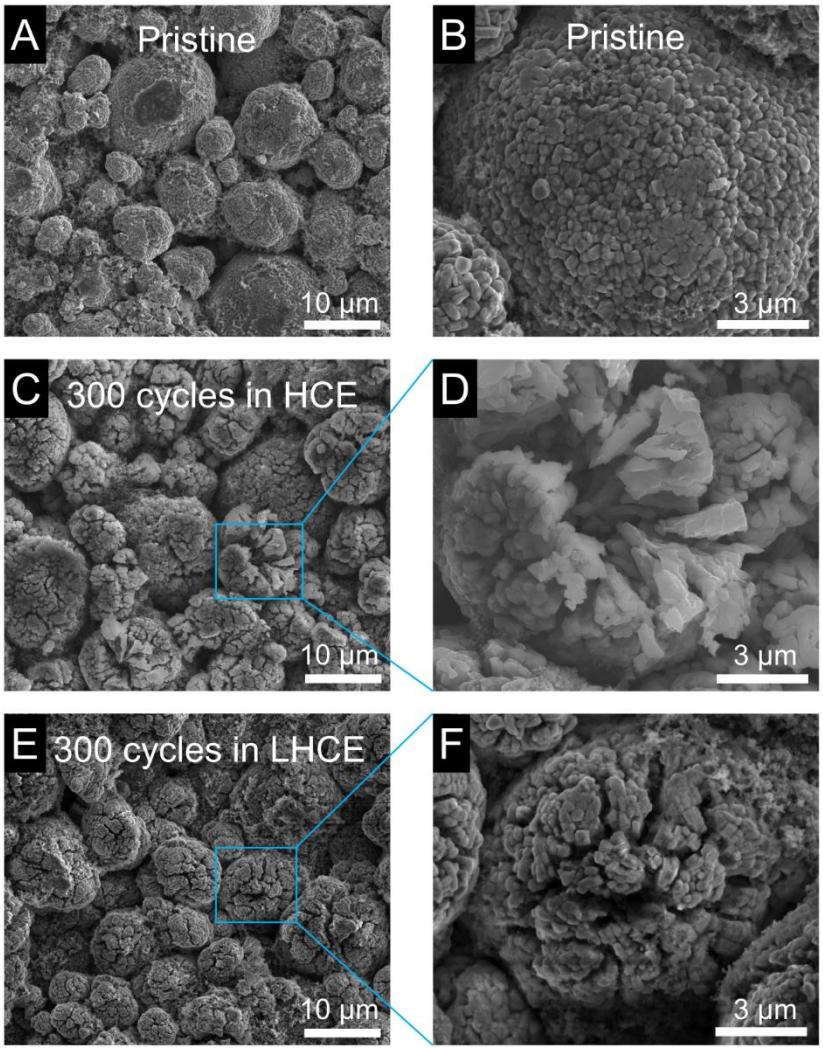

Figure S10. SEM images of the pristine NMC cathode (A, B) and the cathodes after 300 cycles in the HCE (C, D) and the LHCE (E, F).

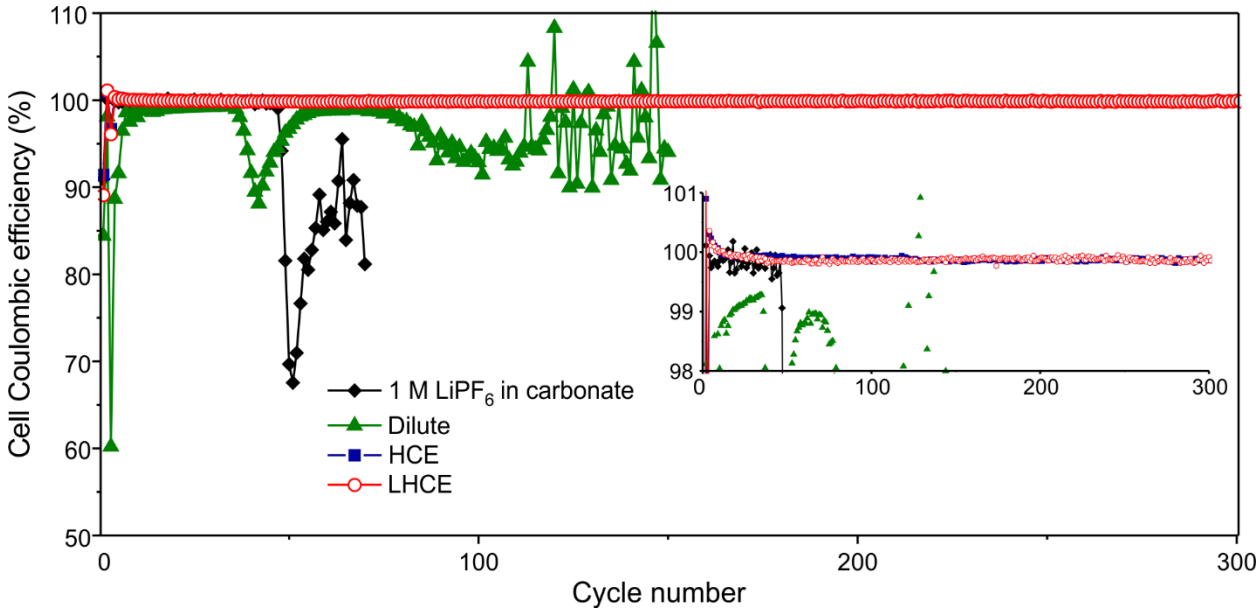

Figure S11. Coulombic efficiencies of Li||NMC cells in different electrolytes.

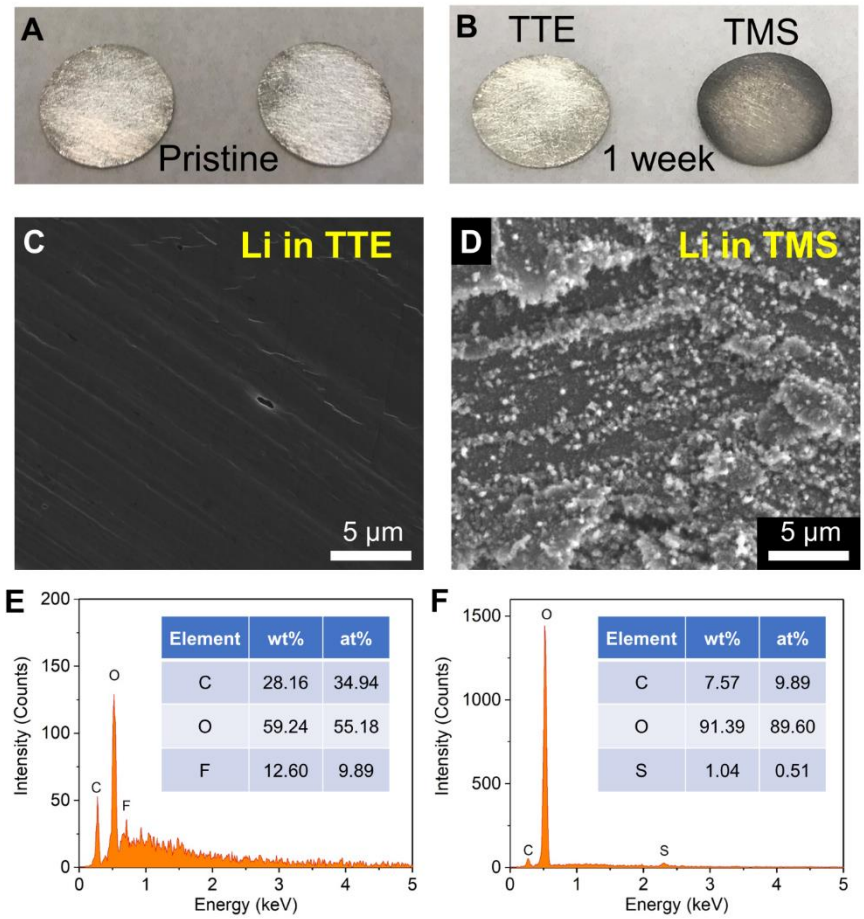

Figure S12. Photos of pristine Li foils (A) and Li foils treated in TTE or TMS (B). SEM images (C, D) and EDX spectra (E, F) of the Li foils treated in TTE and TMS.

Li foils were first mechanically cleaned to remove the initial surface layer and then kept in pure TTE or TMS solvent for 1 week under 50ºC. After this treatment, the Li foil in TTE is still shinny with no apparent roughness change on the Li surface. The EDX spectrum of this Li also indicates a thin surface layer was generated from the reaction between Li metal and TTE. In contrast, the Li foil treated in TMS shows darker color and the SEM image reveals a much rougher surface. The surface layer is also much thicker, as indicated by the strong intensities of signals in EDX.

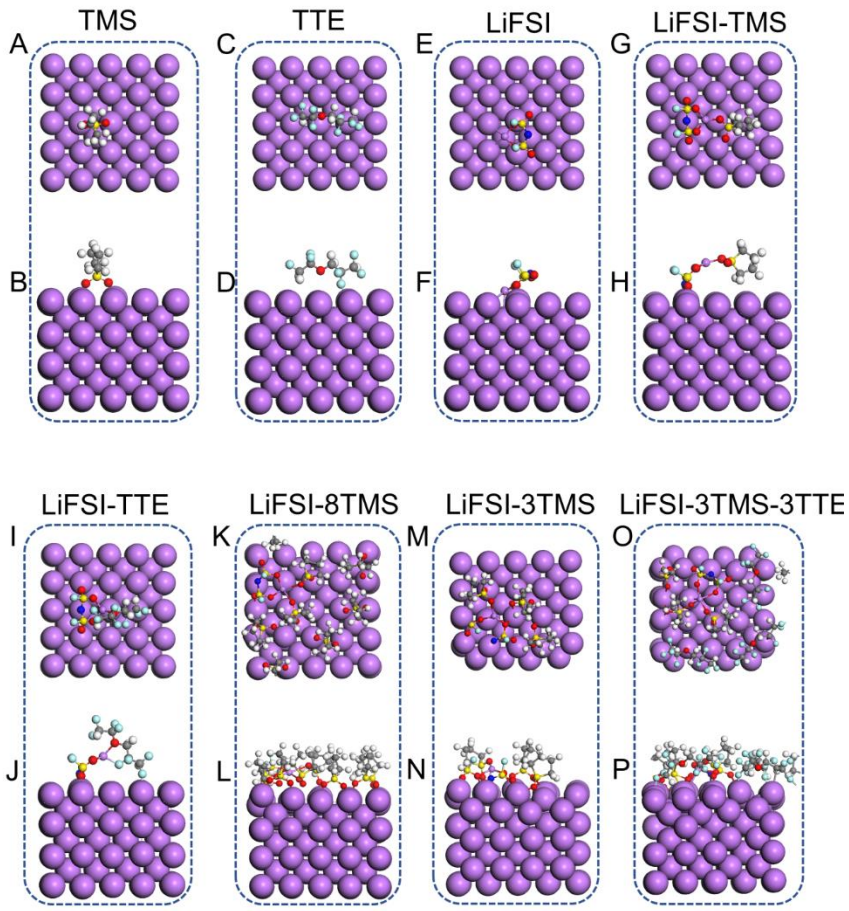

Figure S13. Adsorption of solvent molecules (TMS and TTE), salt (LiFSI) and the salt-solvent pairs (LiFSI-TMS) on the Li(100) anode surface. The upper and lower images are the top and the side view structures.

Table S3. DFT calculated adsorption energies and Bader charges of TMS, TTE, and LiFSI on the Li(100) anode surface

Solvent/salt	Adsorption energy ($kJ \cdot mol^{-1}$)	Bader charge (|e|)
TMS	-80.8	-0.22
TTE	-10.2	-0.10
LiFSI	-87.4	-1.97
LiFSI-TMS	-88.5	-1.38
LiFSI-TTE	-81.5	-1.45
LiFSI+3TMS	-301.5	-2.94
LiFSI+8TMS	-535.2	-4.34
LiFSI+3TMS+3TTE	-464.5	-4.96

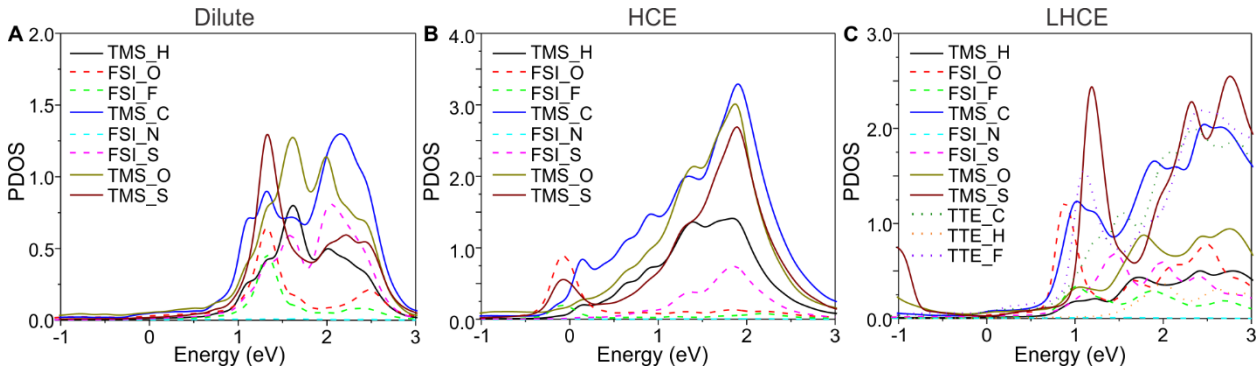

Figure S14. Projected density of states (PDOS) of LiFSI-8TMS (dilute, A), LiFSI-3TMS (HCE, B), and LiFSI-3TMS-3TTE (LHCE, C) on the Li(100) anode surface.

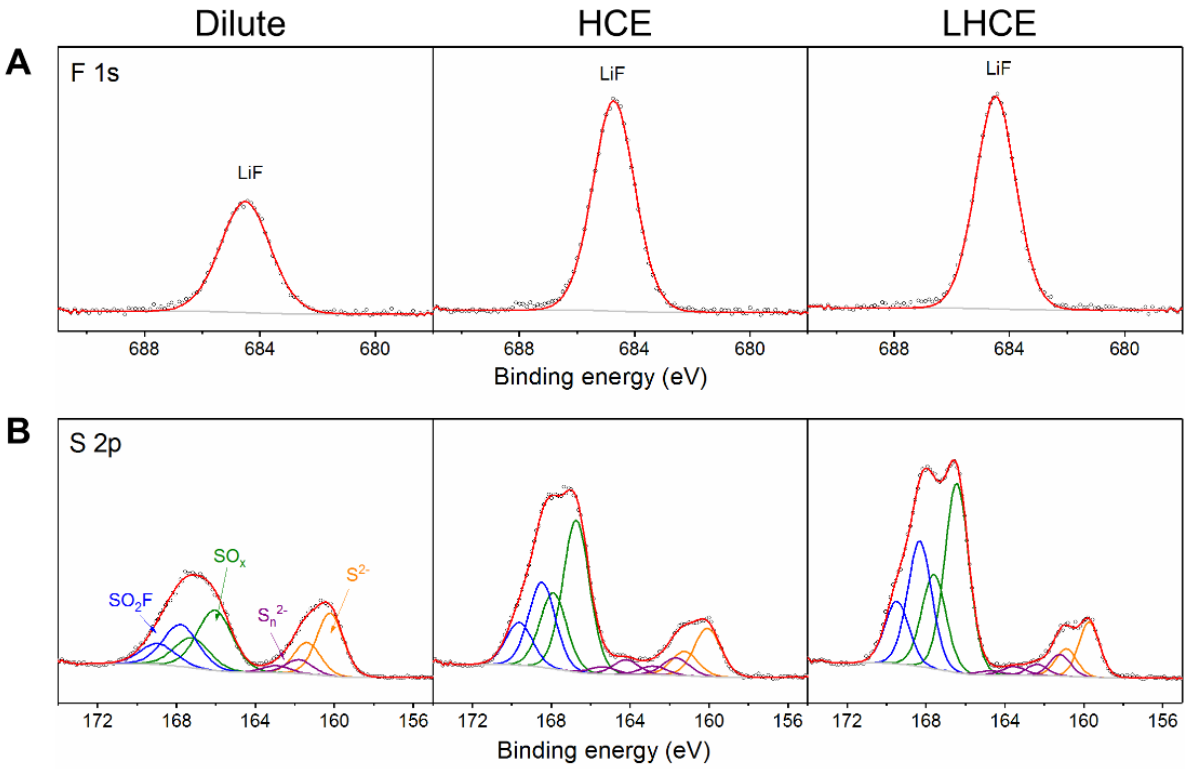

Figure S15. F 1s (A) and S 2p (B) XPS spectra of the Li SEI layers formed in different sulfone-based electrolytes (sputtering depth=0 nm).

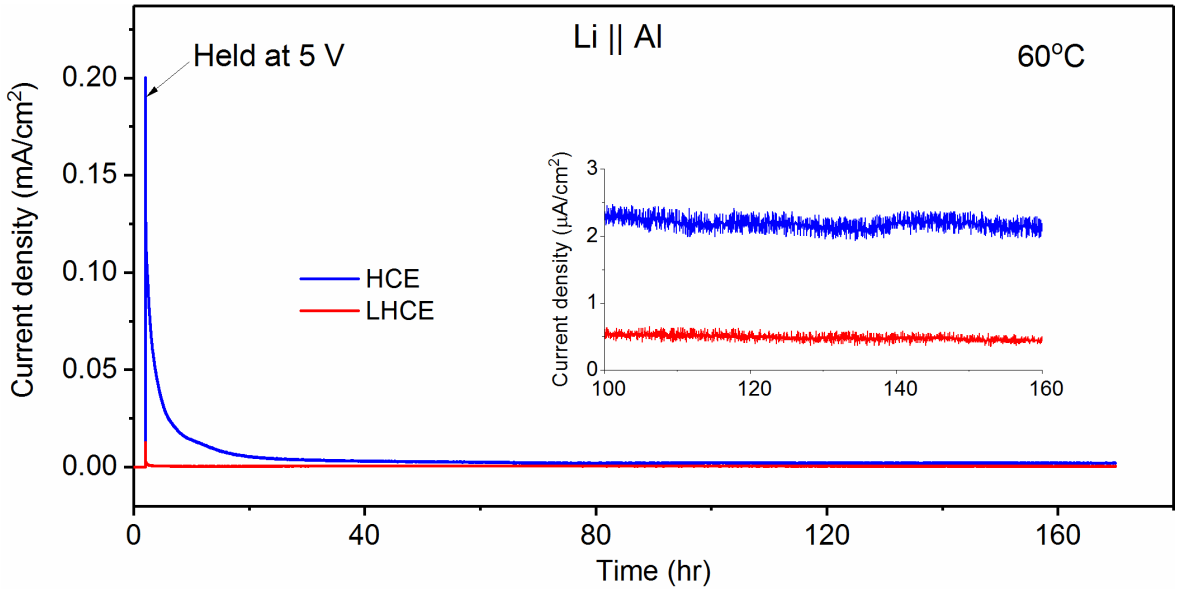

Figure S16. Chronoamperometry in the HCE and the LHCE at 5 V on an Al foil in Li||Al coin cells under 60°C.

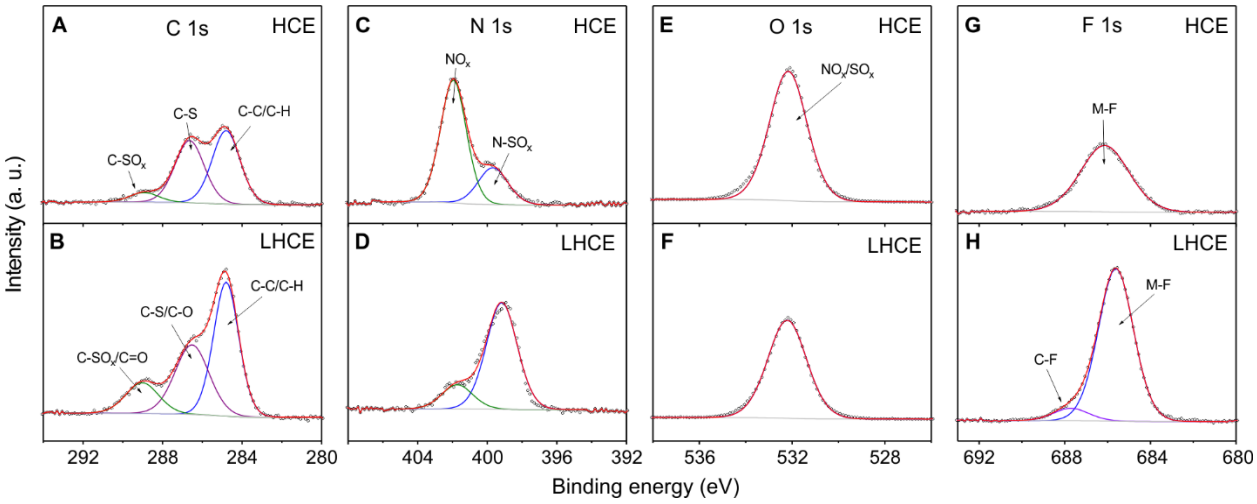

Figure S17. The C 1s (A, B), N 1s (C, D), O 1s (E, F), and F 1s (G, H)XPS spectra of Al foils after held at 5 V for 7 days in the HCE and the LHCE at 60°C.

In the HCE electrolyte, the species on the Al foil are mostly derived from the TMS solvent and the LiFSI salt, as indicated by the C-SO_x, C-S, NO_x, SO_x and fluoride signals (Figure S17). Although similar signals are also found on the Al foil surface tested in the LHCE electrolyte, apparently stronger C 1s (likely more C-C/C-H, C-O and C=O species) and fluoride (F 1s) signals as well as a new C-F signal (F 1s) were observed, which implies the involvement of TTE in the passivation layer formation. At the same time, a higher ratio of N-SO_x/NO_x signals in the N 1s spectra was seen with the addition of TTE, which also indicates the oxidative decomposition of LiFSI was inhibited.

Reference

1. Frisch, M.J.T., G. W.; Schlegel, H. B.; Scuseria, G. E.;, Robb, M.A.C., J. R.; Scalmani, G.; Barone, V.; Mennucci, & B.; Petersson, G.A. et al. Gaussian 09; Gaussian, Inc.: Wallingford, CT. (2009).